REVIEW

Confocal scanning optical microscopy and its applications for biological specimens

DAVID M. SHOTTON

Department of Zoology, University of Oxford, South Parks Road, Oxford OX1 3PS, England

Summary

Confocal scanning optical microscopy (CSOM) is a new optical microscopic technique, which offers significant advantages over conventional microscopy. In laser scanning optical microscopy (SOM), the specimen is scanned by a diffraction-limited spot of laser light, and light transmitted or reflected by the in-focus illuminated volume element (voxel) of the specimen, or the fluorescence emission excited within it by the incident light, is focused onto a photodetector. As the illuminating spot is scanned over the specimen, the electrical output from this detector is displayed at the appropriate spatial position on a TV monitor, thus building up a two-dimensional image.

In the confocal mode, an aperture, usually slightly smaller in diameter than the Airy disc image, is positioned in the image plane in front of the detector, at a position confocal with the in-focus voxel. Light emanating from this in-focus voxel thus passes through the aperture to the detector, while that from any region above or below the focal plane is defocused at the aperture plane and is thus largely prevented from reaching the detector, contributing essentially nothing to the confocal image. It is this ability to reduce out-of-focus blur, and thus permit accurate non-invasive optical sectioning, that makes confocal scanning microscopy so well suited for the imaging and three-dimensional tomography of stained biological specimens.

In this review, I explain the principles of scanning optical microscopy and blur-free confocal imaging, discuss the various imaging modes of confocal microscopy, and illustrate some of its early applications.

Key words: cellular tomography, confocal microscopy, fluorescence microscopy, immunofluorescence, out-of-focus blur removal, optical sectioning, scanning optical microscopy, three-dimensional imaging.

Introduction

Conventional epi-fluorescence microscopy, widely used for the immunocytochemical localization of cellular antigens within permeabilised cultured cells and frozen sections of biological tissue, suffers from one major disadvantage, namely out-of-focus blur. The illumination of the entire field of view of the specimen with intense light at the excitatory wavelength (Fig. 1A) excites fluorescence emissions throughout the whole depth of the specimen, rather than just at the focal plane. Much of the emitted light coming from regions of the specimen above and below the focal plane is collected by the objective lens and thus contributes as out-of-focus blur to the final image of the specimen at that focal plane, seriously degrading it by reducing the contrast and sharpness of the image. This explains why studies by conventional immunofluorescence microscopy of cytoskeletal organization are most informative on well-flattened cultured cells, and why the maximum usable thickness of frozen tissue sections for immunofluorescence observations is about 10 μm. Similar, although less severe, image degradation, due to out-of-focus regions of the specimen, is experienced in other conventional imaging modes, particularly phase-contrast microscopy. This being the case, it would be highly desirable if an alternative method were available that yielded optical microscopic images intrinsically free from out-of-focus blur.

Confocal scanning optical microscopy (CSOM) has recently emerged as the precise solution to this requirement, giving images in which out-of-focus blur is essentially absent. It has several additional advantages over conventional optical microscopy, including the possibility of a significant improvement in lateral resolution and the capability for direct non-invasive serial optical sectioning of intact and even living specimens. Such cellular tomography by CSOM is able to provide high-resolution digitized data sets of the three-dimensional

Journal of Cell Science 94, 175–206 (1989)

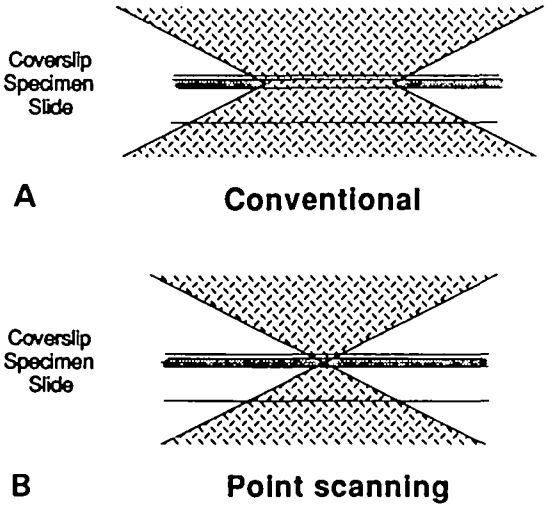

Fig. 1. A comparison of the illumination experienced by the specimen during: A, full-field epi-illumination in a conventional fluorescence microscope; and B, single voxel illumination at the focal plane by a diffraction-limited point of light in a unitary beam laser scanning optical microscope, both employing an oil-immersion objective lens of high numerical aperture. The volume occupied by the specimen between the coverslip and the microscope slide is stippled, and the cone of illuminating light is shown cross-hatched. For simplicity, refraction effects are not shown.

(3-D) distribution of labels within cells or tissue, suitable for subsequent image processing.

While confocal scanning fluorescence microscopy (CSFM) is presently the most important imaging mode of the scanning optical microscope (SOM) for biological specimens, it may also be used in other optical modes, including confocal reflection contrast and transmission imaging, the former being particularly useful for imaging the light reflected by colloidal gold immunoconjugate labels. These alternative imaging modes are described below, following a discussion of image formation and confocal out-of-focus blur removal in the scanning optical microscope.

Image formation in the scanning optical microscope

The scanned image

Scanned image microscopy may be divided into two fundamentally distinct types. Image plane scanning encompasses all forms of microscopy in which the two-dimensional optical image of the specimen is focused conventionally onto the image plane of an electronic imaging device, such as the faceplate of a conventional video camera image tube or the semiconductor array of a charge coupled device (CCD) array camera, from which it is read out, by the raster scanning of the faceplate or the sequential charge transfer of the CCD array, as a series of sequential image lines. I have discussed biological applications of this form of scanned image microscopy in a previous review (Shotton, 1988*a*).

By contrast, scanning optical microscopy (SOM) involves *object plane scanning*. In this, a two-dimensional optical image of the specimen is *not* formed within the microscope, but rather the specimen itself is scanned by a focused spot of light, and the result of the interaction of the light with successive areas of the specimen is recorded using a non-imaging photodetection device such as a photodiode or photomultiplier tube. SOM is thus the optical equivalent of scanning electron microscopy (SEM).

SOM is a relatively new microscopical technique, initially pioneered by relatively few research groups. The only previous review of the subject is that by Sheppard (1987). Pre-1986 publications in this field known to me, ordered by year of first publication, are: Minsky, 1957, 1988; Egger and Petran, 1967; Petran *et al.* 1968, 1985*a*,*b*; Sheppard and Choudhury, 1977, 1978; Brakenhoff *et al.* 1978, 1979, 1980, 1981, 1985; Cremer and Cremer, 1978; Sheppard and Wilson, 1978*a*,*b*,*c*; Brakenhoff, 1978, 1979; Ash, 1980; Sheppard, 1980, 1982; Wilson, 1980, 1981, 1985*a*,*b*; Wilson *et al.* 1980; Bartels *et al.* 1981; Hamilton *et al.* 1981, 1984; Cox *et al.* 1982*a*,*b*,*c*; Hamilton and Wilson, 1982*a*,*b*, 1984*a*,*b*; Shoemaker *et al.* 1982; Wilson and Hamilton, 1982, 1984; Boyde *et al.* 1983; Cox and Sheppard, 1983*a*,*b*; Deinet *et al.* 1983; Sheppard and Hamilton, 1983, 1984; Cox, 1984; Sheppard and Heaton, 1984; Wilson and Sheppard, 1984; Boyde, 1985*a*,*b*; Brearley, 1985; Carlsson *et al.* 1985; Howard *et al.* 1985; Kalish *et al.* 1985; van der Voort *et al.* 1985; Wijnaendts van Resandt *et al.* 1985; Wilke, 1985. Some of these publications are not separately referenced in the subsequent text, but are included here to provide a comprehensive bibliography of the origins of this technique. Many of the initial applications of SOM were in the materials and semiconductor fields, but its suitability for the observation of transparent three-dimensional biological specimens is now universally appreciated.

In SOM, an objective, usually of high numerical aperture, is used to focus a beam of laser light to a single diffraction-limited point or in-focus volume element (voxel) within a three-dimensional specimen. This is commonly achieved by arranging for the laser beam to illuminate an aperture or pinhole situated at the primary image plane of the microscope objective lens, and allowing the objective to image and demagnify the light transmitted by this illuminating aperture into the microscope's focal plane within the specimen (Fig. 1B). Such an instrument is known as a unitary beam SOM, to distinguish it from an alternative design of instrument, the tandem scanning reflected light microscope (TSRLM), discussed below, in which the specimen is simultaneously scanned by many focused light beams. In the epi-illumination configuration of a unitary beam SOM, the same objective is then used, in conjunction with an appropriate beam splitter or dichroic mirror, to image the reflected light or fluorescence emission from the specimen onto the photodiode or photomultiplier tube (PMT) light detector (Fig. 2). Alternatively, the SOM may be used in a transmission mode, in which a second lens is used to image the light to the detector.

To produce an image using a SOM, as with any

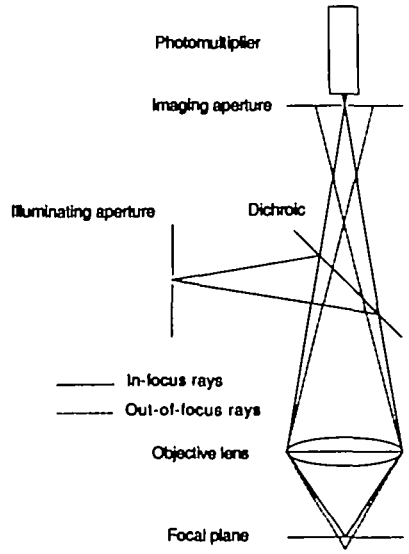

Fig. 2. The confocal principle in epi-fluorescence scanning optical microscopy. Excitatory laser light from the illuminating aperture passes through an excitation filter (not shown), is reflected by the dichroic mirror and is focused by the microscope objective to a diffraction limited spot at the focal plane within the specimen. Fluorescence emissions, excited both within the illuminated in-focus voxel and within the illuminated cones above and below it (shown in Fig. 1B), are collected by the objective and pass through the dichroic mirror and the emission filter (not shown). However, only those emissions from the in-focus voxel (——) are able to pass unimpeded through the imaging aperture to be detected by the photomultiplier. Fluorescence emissions from regions below the focal plane (– – –) and from above it (not shown) have different primary image plane foci and are thus severely attenuated by the imaging aperture, contributing essentially nothing to the final confocal image.

scanning microscope, the illuminating point probe must be moved in a regular two-dimensional raster across or, more accurately for transparent three-dimensional biological preparations, *through* the specimen, and the instantaneous response of the light detector at all points in this scan must be displayed with equivalent spatial position and relative brightness on the synchronously scanned phosphor screen of a CRT monitor or on some other suitable imaging device. The image is thus built up point by point, as on the screen of an SEM monitor or of a domestic television, although the scanning rate for SOM is usually significantly slower than the 25 or 30 frames per second of conventional video. In contrast to a conventional light-microscopic image or a photographic record of one, the temporally linear analogue electronic signal produced by the light detector while acquiring a SOM image is easy to digitize 'on the fly' and accumulate in a digital image memory (frame store), from which it may be read out and displayed at video rates. It is thus ideally suited for subsequent digital image processing, for instance to enhance the contrast or sharpen the edges within the image obtained (Cox, 1982; Cox and Sheppard, 1983*a*,*b*; Hamilton and Wilson, 1984*b*; Wilson and Sheppard, 1984; Robert-Nicond *et al.* 1989; Schormann *et al.* 1989; van der Voort *et al.* 1989).

Early SOMs often for convenience used helium–neon lasers emitting red light of 633 nm wavelength, but most instruments today are fitted with a low-power air-cooled argon ion laser. In the 'all lines' mode, this laser emits a variety of wavelengths, of which the two strongest lines are at 488 nm, at the excitation maximum of fluorescein, and at 514 nm, capable of exciting fluorescence emissions from rhodamine and Texas Red, thus making it suitable for use with the most commonly used biological fluorochromes employed in immunocytochemistry. More expensive lasers emitting at other wavelengths, particularly tunable dye lasers emitting in the ultraviolet, may also be fitted to meet particular requirements.

Modes of image formation

In practice, scanning of the laser beam may most conveniently be brought about either by the lateral movement of the specimen in the focal plane relative to a stationary optical path (scanned stage SOM), or by the angular movement of the illuminating beam filling the back focal plane of a stationary objective, which causes the focused light beam to move laterally in the focal plane relative to the stationary specimen (scanned beam SOM).

Scanned stage SOM, first developed by Sheppard and his colleagues (Sheppard and Choudhury, 1977; Sheppard and Wilson, 1978*a*,*b*; Wilson, 1980, 1985*a*, 1986; Wilson and Sheppard, 1984; Sheppard, 1987), has been the method used for most prototype SOMs built in research laboratories (Wijnaendts van Resandt *et al.* 1985; Brakenhoff *et al.* 1979, 1980, 1986, 1989; Brakenhoff, 1979; van der Voort *et al.* 1985, 1987, 1988). It has the important advantage of constant axial illumination, thus reducing optical aberrations and ensuring complete evenness of optical response across the entire scanned field (space-invariant imaging), a feature desirable for optimal image quality and ease of subsequent image processing. In addition, it permits scanned fields of view much larger than the static field of view of the objective employed, and thus allows one to change between very low and very high magnification imaging while maintaining optimal resolution and light-collection, by the simple expedient of altering the stage scan amplitude while using a single high-magnification objective of high numerical aperture. However, because of physical limitations of the speed of accurate two-dimensional stage scanning, these microscopes generally have a slow scan rate, usually taking at least 10 s to collect a high-quality image of 512^2 pixels (digitized picture elements), although this time may be reduced proportionately by scanning a smaller pixel field (Brakenhoff *et al.* 1986; van der Voort *et al.* 1988). Such instruments, now in commercial production and primarily used for materials and semiconductor applications (Dixon and Martin, 1986), are purpose-built electronic imaging devices, physically resembling small scanning electron microscopes, and lack the alternative capability for direct conventional full-field optical microscopic viewing of the specimen through eyepieces.

Scanned beam SOM (Wilke, 1985; Carlsson *et al.* 1985; Carlsson and Åslund, 1987; White, J.G. *et al.*

1987; Takamatsu and Fujita, 1988; Carlsson and Liljeborg, 1989), in which rotating or vibrating mirrors cause angular scanning of an expanded beam of light filling the aperture of the back focal plane of a plan (flat field) objective, usually allows higher scanning frame rates, of between 0.1 and 2 Hz for an image of 512^2 pixels. Suzuki and Horikawa (1986) and Horikawa *et al.* (1987) have reported the development of a real-time laser scanning optical microscope operating in transmission and reflection non-confocal differential phase-contrast modes, Draaijer and Houpt (1988) have developed a similar but confocal reflection and epi-fluorescence scanning microscope, and Goldstein (1989) has recently reported a 'no moving parts' confocal reflection/transmission confocal scanning microscope employing an image dissector tube for image detection, in all of which rapid beam scanning is achieved by the use of acousto–optic deflectors, giving image readout at standard video rates (25 or 30 frames per s).

The use of acousto–optic deflectors is reported to introduce small geometric and intensity distortions into the image, which at present can be corrected for only partially (Horikawa *et al.* 1987). In addition they lead to a further problem for confocal fluorescence imaging, since the longer-wavelength fluorescence emission cannot be descanned back through the wavelength-specific acousto–optic modulator. Two solutions to this have been proposed, in both of which scanning and descanning along the slower (y) axis is brought about conventionally by mirrors. One is to project the partially descanned fluorescence emission signal onto a linear array of CCD detectors, which are read out in synchrony with the x scan, thus obviating the need to descan the beam physically (Awamura *et al.* 1987). The other is to image the partially descanned fluorescence emission through a slit, rather than a circular, confocal imaging aperture. Wilson (1989) discusses the degree to which this method compromises the true confocality and out-of-focus blur rejection of the image obtained. Despite these limitations, such fast-scanning instruments represent a significant advance, removing one of the principal limitations of other forms of unitary beam SOM and permitting the use of scanning optical microscopy for the study of dynamic processes in living cells, or the rapid automatic screening and analysis of large areas of cytological or haematological specimens. The usefulness of video-rate scanning systems for fluorescence microscopy is still debatable, however, since at high magnification a low fluorescence signal may require the subsequent integration of several video frames to achieve a satisfactory signal-to-noise ratio, thereby giving no advantage over a slow-scan system.

In the most advanced development for cytology, Bartels *et al.* (1981) and Shoemaker *et al.* (1982) described the construction of an ultrafast autofocusing laser scanning microscope, which is a hybrid between a scanned stage and a scanned beam instrument. In this, a rotating polygonal mirror is used to scan the beam rapidly in the x direction through a custom-made 10 cm diameter 0.8 NA objective having a field of view and thus a scan width of 2 mm. By physically translating the specimen beneath the objective in the y direction, in 10 sequential parallel lines 20 mm long and spaced 2 mm apart, an image of a 20 mm by 20 mm specimen area is generated every 60 s, composed of 40 000 by 40 000 pixels each 0.5 μm by 0.5 μm area, with a pixel measurement frequency of 64 MHz.

As in conventional optical microscopy, the image field of view in conventional scanned beam SOMs, in which the specimen is not moved, is limited to that of the objective used, but this tends to be less of a problem for many biological specimens than it is for materials or semiconductor applications. The great practical advantage of this type of SOM for the biologist is that it may be achieved by direct attachment of a scanning unit to an existing conventional compound microscope, enabling all the normal full-field imaging modes (bright and dark field, phase-contrast, Nomarski DIC, conventional epi-fluorescence, reflection contrast, etc.) to be retained and employed on the same specimen.

The relatively slow scan rate of most SOMs, which means that the result of refocusing the image is not seen instantaneously, in the way to which we have become accustomed using conventional microscopes, and the absence of out-of-focus fluorescence information, described below, make it sometimes difficult and tedious to locate and focus upon a fluorescent specimen consisting of scattered discrete objects, such as cultured cells on a coverslip, by inspection of the confocal fluorescence image alone, since such objects are completely invisible when out-of-focus! In these cases it is particularly useful to be able to use conventional viewing modes prior to confocal scanning fluorescence microscopy. This limitation is removed when using a video-rate scanning confocal microscope (Draaijer and Houpt, 1988).

A third alternative method of scanning a single beam across the specimen is that of scanning the objective itself, relative to a stationary specimen and a stationary illuminating system. While suffering from a number of optical disadvantages, this method has been practically implemented by Hamilton and Wilson (1986) on an optical bench, and by Reimer *et al.* (1987), who substituted an optical objective for the acoustic lens in a modified Leitz ELSAM scanning acoustic microscope.

The final logical possibility for scanning is that of scanning the illuminating aperture, or more accurately a very large array of apertures, relative to a stationary optical beam, a stationary objective and a stationary specimen. This is the method employed in the other main type of SOM, the tandem scanning reflected light microscope (TSRLM), which has been described and discussed by Egger and Petran (1967), Petran *et al.* (1968, 1985*a*,*b*, 1986), Sheppard and Wilson (1981), Boyde *et al.* (1983, 1986), Boyde (1985*a*,*b*, 1986, 1987), and Lewin (1985). In this instrument, scanning is brought about by the high-speed rotation, in the primary image plane of the objective, of a Nipkow disc containing several thousand pairs of diametrically opposed apertures arranged in Archimedean spirals, such that together, when rotated, their demagnified images cover the entire field of view of the objective.

The TSRLM differs in five fundamental respects from the scanned stage, scanned beam and scanned objective

unitary beam SOMs mentioned above. First, since the whole image is scanned many times a second, the microscope yields a stable, apparently continuous image, which can be viewed through an eyepiece in real time, as in any conventional light microscope. It can thus be used to study rapidly moving living specimens. Second, since a broad-spectrum non-coherent (white light) light source may be used, rather than a monochromatic laser, images may be obtained which have natural colour. Third, the Nipkow disc situated in the optical path typically transmits only 1% of the light incident upon it (Petran *et al.* 1985*a*). Thus, when used for epi-fluorescence microscopy, the TSRLM may require the attachment of an intensifying video or CCD camera to achieve a satisfactory signal level. Fourth, like that from any conventional optical microscope, the visual image is not immediately available as an electronic signal, although it may readily be converted into one by such a camera. This permits video-rate digital image processing, for instance, to enhance the image contrast or to average successive frames in order to improve the signal-to-noise ratio of fluorescent images. Finally, the optical design does not permit direct x,z vertical sectioning (discussed below).

Almost all the TSRLMs in use today are of the original Petran design (Egger and Petran, 1967; Petran *et al.* 1968), in which illuminating light passes down to the specimen through one set of apertures, while reflected or fluorescently emitted light passes back up to the eyepiece not through these same apertures but *via* the diametrically opposed ones on the opposite side of the Nipkow disc, having been separated from the illuminating beams by a beam splitter. However, Xiao and Kino (1987) and Xiao *et al.* (1988) have recently reported the development of a variation of the TSRLM, which they call the spiral scanning optical microscope (SSOM), in which both transmitted and reflected light beams pass through the *same* set of apertures. This arrangement is reported to simplify the mechanical construction of the microscope, and thus to reduce the alignment problems to which the original design is prone. In addition, their Nipkow disc is made from a glass plate bearing a black emulsion photomask, which permits smaller and more accurately positioned apertures than the physical holes in the thin copper sheet of Petran's original Nipkow disc, and thus more nearly achieves the enhanced spatial resolution characteristic of confocal microscopes, discussed below. This disc bears 150 000 apertures of 20 μm diameter arranged in 16 spirals, of which 4000 transmit light to the specimen at any one time. The disc is rotated at 2400 revs min^{-1}, and generates an apparently continuous *circa* 7000 line image at 640 frames per s, with an observed two-point spatial resolution of 400 nm. Unwanted light reflected from the Nipkow disc itself is eliminated from the image in several ways: by use of the matt black finish on the disc, which reflects only 4% of the incident light; by using a convergent, rather than a parallel, illuminating beam, with a small black mask at the focal point of the reflected image of the light source (or, most recently, by inclining the disc slightly so that light is reflected off-axis); and by employing the antiflex principle of reducing unwanted reflections (Piller, 1959; Ploem, 1975), with a polarizer in the illumination path, a crossed analyser in the imaging path, and a quarter-wave plate below the Nipkow disc, the effect of which is to rotate by 90° the plane of polarization of the light reflected by the specimen itself, so that it may pass the analyser. Although Xiao *et al.* (1988) had not at that time implemented this modification, it is obvious that by replacing the beam splitter and antiflex components of their system with a conventional fluorescence filter block consisting of a dichroic beamsplitter and selective excitation and emission filters, their instrument would be equally suitable for fluorescence imaging, albeit with the reduced intensity characteristic of Nipkow disc systems.

For clarity, and since the TSRLM has been well reviewed elsewhere, subsequent discussion in this review is limited to unitary beam SOMs

Computational requirements

While it is entirely feasible to operate a scanning optical microscope as an entirely analogue instrument, the suitability of the unitary beam SOM linear data stream for digitization, and the usefulness of subsequent digital image-processing and image-storage techniques, has resulted in most SOMs being configured as digital imaging systems, interfaced to a small computer, which is also used to control the microscope scanning and image display synchronization. Many of the prototype SOMs and a certain number of commercial instruments are built around dedicated microprocessors. Others, particularly those that can be fitted as accessories to conventional optical microscopes, are interfaced to an industrial standard microcomputer equipped with proprietary scan control and image-processing boards and menu-driven software, making a compact and easy to use stand-alone system for data acquisition and image display.

One important consideration, particularly for three-dimensional imaging, is the amount of digital storage required for confocal images. For high-resolution confocal microscopy, the Nyquist sampling frequency of twice the spatial resolution of the optical system, required to represent exactly an image of the real continuous world by its digitized samples (Castleman, 1979), involves sampling x and y at 100 nm intervals, and z, because of the intrinsically poorer axial resolution even of the confocal microscope (see below), at 400 nm. At this resolution, a single 768×512 pixel confocal image covers an area of approx. 75 μm by 50 μm and requires 0.375 Mbytes of digital image storage. A 3-D voxel image about 50 μm deep, comprising 128 0.4-μm thick x,y optical sections, would occupy 48 Mbytes. For 4-D (x, y, z and time) work on living cells, smaller sub-images must be used, to prevent the storage requirement becoming astronomically large. If, for example, 20 time-points are used and sub-images of only 256×256×64 voxels are selected (i.e. a 25 μm^3 sampled volume), storage for 80 Mbytes of digitized data must be found for *each* experiment. Since it is impracticable to store such data sets on the 40 Mbyte hard disc of a standard microcomputer, it becomes necessary to be able to off-load the digitally encoded images to some form of archive medium, such as a very large Winchester disc (or, less satisfactorily, a

magnetic tape), or a WORM (Write Once, Read Many times) or erasable optical disc, which can hold up to 2 Gigabytes. A convenient alternative solution to this problem for those on tight budgets, until low-cost erasable optical discs come onto the market, is the use of removable erasable 20 Mbyte Bernoulli magnetic discs. These have proved particularly useful for transferring images between distant laboratories using the same confocal imaging system.

Data reduction and data compression procedures, such as run-length encoding, are obviously desirable for such large data sets. Smith *et al.* (1989) recommend the use of the octree representation of 3-D binary or grey-scale image data for compact storage with no loss of information, and Carlsson and Liljeborg (1989) report that approximately twentyfold compression may be achieved by storing suitably filtered and thresholded images using vector representation, in which each voxel is represented by its x,y,z coordinates and its intensity value, despite the fact that each voxel requires four times the storage space, since so much of most images, particularly fluorescence ones, consists of uninteresting background voxels, which may be discarded.

The requirement for sophisticated post-processing of large three-dimensional confocal image data sets (see below) soon outstrips the capabilities of a simple microcomputer, and this type of work is best handled by offloading these images to a more powerful computational workstation with image-processing and stereoscopic display facilities, freeing the microcomputer for the control of the primary task of confocal microscopic image acquisition. For the variety of image-processing computational procedures that may be required, particularly the stereoscopic animation discussed below for 3-D and 4-D confocal images of cellular organization, this workstation should, in its complete configuration, be a general purpose image-processing engine of significant power, memory allocation and temporal bandwidth, with a high-speed image memory and special hardware for stereoscopic image display. The amount of high-speed image memory required for the storage and video-rate output of animation sequences may be appreciated by considering the rotational animation at 5° intervals (72 views) of medium resolution (512^2 pixel) images. To provide the ability to switch between the animation of either of two of the three possible orthogonal rotational viewpoints ('tumble' (x), 'roll' (y) and 'spin' (z)), 36 Mbytes of high-speed image display memory would be required. Time-lapse 4-D animation display may be achieved for a single viewpoint in the same amount of video RAM, by storing the complete animation sequences of two adjacent timepoints at any one time, the first being overwritten by that for the timepoint-after-next while the second is being displayed.

The principles of confocal imaging using a scanning optical microscope

Image formation in a conventional optical microscope

It will be useful for the subsequent discussion to recall some fundamental principles of image formation in the conventional light microscope. The discussion in this section closely follows and condenses the detailed and lucid treatments given by Castleman (1979) and Agard (1984) in the context of their procedures for the computational removal of out-of-focus blur.

The relationship between the three-dimensional specimen and the blurred image of it obtained at any chosen focal plane by conventional microscopy, using a high numerical aperture objective having a narrow depth of field, can be defined mathematically from knowledge of the image formation characteristics of the objective lens. Two mathematical functions define this relationship: the two-dimensional in-focus point spread function, s_i, and the out-of-focus point spread function (or defocus blurring function), s_o (where the subscripts i and o denote in-focus and out-of-focus, respectively). The lens contrast transfer functions (CTFs) are the Fourier transforms of these point spread functions (PSFs), and define the way in which the various spatial frequency components of the object are altered by the optical system.

The in-focus PSF, $s_i(x,y)$, or impulse response of the objective, is the mathematical description of the Airy disc image formed by the objective of an idealised dimensionless point object (an impulse or Dirac delta function) situated on the optical axis in the focal plane of the microscope. This familiar image, of a central maximum surrounded by rings of weaker intensity, results from the inability of the objective lens to collect the highest spatial frequencies of light diffracted by the specimen, since these are scattered through angles greater than α, the maximum acceptance half-angle of the objective. (The numerical aperture (NA) is defined as $\mathrm{NA}=\eta \sin \alpha$, α being maximally 67.5° for an oil-immersion objective with an NA of 1.40, used with immersion oil of refractive index $\eta=1.515$). The image is thus said to be diffraction-limited.

The highest spatial frequency, f_c, that can be accepted by an objective lens using monochromatic light of wavelength λ and an immersion fluid of refraction index η is defined as:

$$f_c = (2\eta \sin \alpha)/\lambda = 2\,\mathrm{NA}/\lambda . \qquad (1)$$

Rayleigh's criterion for the resolution limit of the optical microscope, $d_{min_{\mathrm{Rayleigh}}}$, the distance between two point objects at which the peak intensity of the Airy disc of the first object overlaps with the first minimum of the Airy disc of the second, is defined as:

$$d_{min_{\mathrm{Rayleigh}}} = 1.22\,\lambda/2\,\mathrm{NA} = 1.22/f_c , \qquad (2)$$

$d_{min_{\mathrm{Rayleigh}}}$ being 238 nm for light of 546 nm wavelength when using a 1.4 NA objective.

These definitions assume that the objective is receiving light from a condenser of at least equal numerical aperture. If this condition is not fulfilled, the front collecting aperture of the objective will not be fully illuminated and resolution will thereby be impaired, the (2 NA) term in equations (1) and (2) being replaced by $(\mathrm{NA}_{\mathrm{objective}}+\mathrm{NA}_{\mathrm{condenser}})$. In epi-fluorescence and reflection contrast microscopy, of course, the objective also serves as the condenser, satisfying this condition.

The in-focus PSF, $s_i(x,y)$, thus describes the inevitable blurring present in the image, $i(x',y')$, at the primary image plane of the objective, of an infinitely thin in-focus object, $o(x,y)$, using aberration-free conventional optics:

$$i(x',y') = o(x,y) \otimes s_i(x,y)\,, \qquad (3)$$

where $\otimes$ denotes a two-dimensional convolution operation, and the relationship between the coordinates (x,y) and (x',y') is defined by the image rotation and magnification, M, caused by the objective lens: $x'=-Mx$ and $y'=-My$. (Note that for clarity this nomenclature differs from that adopted by Agard (1984), who used o to denote the observed image and i to denote the object.)

Similarly, the out-of-focus PSF, s_o, defines the manner in which this Airy disc image is further degraded when the idealised point object is progressively moved along the microscope's optical axis away from the plane of focus. These two PSFs may be convolved to give the microscope's total three-dimensional PSF, $s(x,y,z)$. The out-of-focus image of the infinitely-thin specimen is thus defined as:

$$i(x',y') = o(x,y) \otimes s_i(x,y) \otimes s_o(x,y,\Delta z) = o(x,y) \otimes s(x,y,\Delta z)\,, \qquad (4)$$

where Δz is the distance of the specimen from the focal plane.

From this it can be shown (Castleman, 1979) that the imaging of a three-dimensional object may also be described by the convolution of the three-dimensional object with the three-dimensional PSF:

$$i(x',y',z') = o(x,y,z) \otimes s(x,y,z)\,. \qquad (5)$$

According to diffraction optics theory, for an ideal lens this three-dimensional PSF should be symmetrical above and below the focal plane, and thus the image should look identical for similar degrees of overfocus and underfocus. In practice, however, using the best high NA objectives to image sub-resolution (100 nm diameter) fluorescent beads, this has been shown to be far from the case (Hiraoka *et al.* 1987). Not only is the PSF strikingly asymmetrical along the z axis, but it also fails to show the expected circular symmetry in planes perpendicular to z. Consequently the three-dimensional PSF must be determined experimentally using sub-resolution point test objects.

Within the three-dimensional CTF, certain image spatial frequencies occupying conical regions above and below the origin ('the missing cones') have zero intensity, resulting in severely impaired spatial resolution along the optical axis of the conventional optical microscope. Thus when optical section images from a conventional optical microscope taken at different focal planes through a three-dimensional object are combined, even after computational deblurring, the overall effect is to blur and elongate the image along the optical axis. Agard (1984) has described the improvements in z resolution that may be obtained by combining different views of the same specimen; for instance, two sets of computationally deblurred optical sections collected along orthogonal axes. The improved resolution of the combined data results from the presence in the second set of sections of spatial frequencies absent from the first, and should be equal in all directions. Such data sets from *Drosophila* embryo nuclei have been successfully collected and combined by Shaw *et al.* (1989), with the expected improvement in resolution.

Exclusion of fluorescence out-of-focus blur in the confocal microscope

In the confocal epi-fluorescence mode of a unitary beam scanning optical microscope (Fig. 2), the fluorescent light emitted by excited fluorochrome molecules in the single diffraction-limited illuminated in-focus voxel is imaged through the same objective *via* a dichroic mirror and suitable interference filters to an aligned imaging aperture at the primary image plane of the objective, and hence to a photomultiplier tube (Brakenhoff, 1979; Cox, 1984). In this arrangement, which is one of the 'type 2' forms of SOM in the nomenclature of Sheppard and Choudhury (1977), the confocality of the imaging aperture with the in-focus voxel ensures that only light emanating from that voxel is fully passed by the imaging aperture and detected by the PMT. In contrast, fluorescence emissions excited by the illuminating beam within the conical illuminated regions of the specimen above and below the in-focus voxel (Fig. 1B) come to focus elsewhere. Light from these regions of the specimen is defocused at the imaging aperture plane, and is thus almost totally prevented by the confocal imaging aperture from reaching the PMT detector (Fig. 2), contributing essentially nothing to the final image. As a consequence, only in-focus information is recorded. While fewer photons reach the detector than without the confocal imaging aperture, it is primarily noise that is lost, rather than signal. Thus the use of a high-sensitivity PMT enables the technique to be used in situations where the fluorescence emission intensity of the specimen is only moderate, or where the intensity of fluorescence excitation is intentionally limited to reduce the rate of photobleaching. If the confocal aperture is removed, all of the defocused light is permitted to reach the photodetector, and depth discrimination is thereby abolished, the imaging properties of the non-confocal ('type 1') SOM being equivalent to those of a conventional light microscope.

Image formation in transmission, reflection and fluorescence confocal microscopy

While in conventional microscopy the image formation is determined by the PSF of the imaging objective, in a confocal SOM the image formation is determined by the PSFs of both the illuminating and the imaging lenses (condenser L1 and objective L2, respectively). This is because both lenses now play an equal role in image formation, the former in defining the size of the diffraction-limited in-focus illuminating voxel and the latter in imaging this to the point detector (Cox *et al.* 1982*a*). The confocal system in-focus PSF is thus the product of the individual PSFs of the two lenses, and the confocal image

is defined by the convolution of the object with this product:

$$i(x',y',z') = o(x,y,z) \otimes (s_{L1}(x,y,z) \cdot s_{L2}(x,y,z)) . \quad (6)$$

For the confocal epi-illumination arrangement (Fig. 2) these two PSFs are, of course, identical, since the same objective is employed for both illumination and imaging. The confocal system PSF thus equals the PSF of the objective lens *squared*.

As for confocal epi-fluorescence imaging described above (Fig. 2), the same basic in-focus selection principle applies when the SOM is operated with a confocal imaging aperture both in transmission and in the reflection contrast mode (in which a simple beamsplitter is substituted for the dichroic mirror). However, there is a fundamental distinction between these two imaging modes and confocal fluorescence imaging. The use of an ideally small circular confocal imaging aperture causes the photomultiplier to function as a coherent point detector. Since the illuminating light is also coherent, the confocal microscope thus acts as a coherent microscope for transmitted and reflected light. In contrast, since fluorescence emissions are by their nature incoherent, the confocal fluorescence microscope is an incoherent imaging system. This has implications for spatial resolution, discussed below, since in theory incoherent imaging should yield higher axial and lateral spatial resolution.

Furthermore, confocal imaging of fluorescence emission involves an additional fundamental difference. Fluorescence emission generally occurs at a longer wavelength than that of the excitation, by a factor determined by the Stokes' shift of the particular fluorochrome employed. The spatial resolution of confocal fluorescence imaging will thus be determined both by the illuminating wavelength (λ_1) and by the emission wavelength (λ_2), since in the confocal system it is the shorter wavelength excitatory light, λ_1, which determines the size of the illuminated voxel. Thus in CSFM the highest spatial frequency that can be recorded is proportional to $(1/\lambda_1 + 1/\lambda_2)$, the image obtained being defined by:

$$i(x',y',z') = o(x,y,z) \otimes (s_{\lambda 1}(x,y,z) \cdot s_{\lambda 2}(x,y,z)) . \quad (7)$$

This gives the confocal scanning microscope, when used in fluorescence mode, an *additional* resolution advantage over the conventional fluorescence microscope, in which the spatial resolution is determined solely by the longer wavelength, λ_2, of the fluorescence emission (Cox *et al.* 1982*a*; Cox, 1984; Wilson and Sheppard, 1984; Sheppard, 1986*a*; Wilson, 1989). Since resolution decreases with increasing wavelength, choice of fluorochromes with shorter excitation wavelengths and smaller Stokes' shifts will maximise the spatial resolution of the images obtained.

Enhancement of axial resolution

There are various ways of enumerating the depth discrimination properties of the scanning optical microscope and of estimating the improvement in axial resolution brought about by confocal imaging, in comparison with a conventional microscope or with a SOM that is operated without a confocal imaging aperture (a 'type 1' SOM, in the nomenclature of Sheppard and Choudhury, 1977), which is optically equivalent. These are based on the modelling and the experimental determination of the imaging of a variety of theoretical object forms and actual test specimens (points, lines, planes and extended structures), which serve, e.g. as models for single immunogold labels in a cell surface, for fluorescently labelled filamentous cytoskeletal structures and planar membranes, and for more complex cellular structures (Sheppard and Wilson, 1978*b*; Hamilton *et al.* 1981; Wilson and Sheppard, 1984; Corle *et al.* 1986; Wilson and Carlini, 1987*b*, 1988, 1989; Brakenhoff *et al.* 1989; Sheppard, 1987, 1989).

The more recent of these publications have been particularly helpful in relating theoretical predictions to experimental results, and in addressing practical considerations such as the use of high NA objectives (many of the early theoretical calculations assumed a relatively low NA), the size and shape of the confocal imaging aperture used, and the effects of optical aberrations in the objective lens. Indeed, by imaging a plane mirror surface, it has been shown that the confocal reflection microscope is the ideal tool to quantify the degree of astigmatism and spherical aberration in one's objectives (Sheppard and Coggiswell, 1989; Wilson and Carlini, 1989).

One measure of axial resolution is to consider the decrease in the axial image intensity of an idealised point object situated on the optical (z) axis, as one adjusts the focus of the microscope to move the object away from the focal plane. Using the formulae developed by Born and Wolf (1975) to define the PSF of the objective lens, in a confocal microscope with an ideally small confocal imaging aperture, the axial intensity of the image of an ideal point object can be calculated at differing degrees of defocus. From this it can be shown that the depth of field of a confocal microscope, defined as the half-width of this function, is reduced relative to that of a non-confocal microscope by a small but significant factor of about 1.4 (Sheppard and Wilson, 1978*b*; Corle *et al.* 1986; Brakenhoff *et al.* 1989). Theoretical considerations (Carlsson and Åslund, 1987) dictate that this confocal axial resolution will always be about three times poorer than the optimal confocal lateral resolution, discussed below. Because of the double effect of the illuminating and imaging lenses (eqn (6), above), this confocal increase in axial resolution is inversely proportional to the *square* of the numerical aperture of the objective employed in a confocal epi-illumination system, making it imperative to use objectives of the highest NA to obtain high confocal z resolution.

The most fundamental measure of resolution is the spatial frequency cutoff of the imaging system's optical transfer function. On the basis of this criterion, and the fact that fluorescence emissions are incoherent relative to the illuminating coherent light, Sheppard (1989) confirmed the long-established conclusion (Cox *et al.* 1982*a*; Wilson and Sheppard, 1984) that the maximum axial and lateral spatial frequencies transmitted by confocal fluorescence imaging should be twice those of a conventional

incoherent fluorescence microscope, assuming a Stokes' shift of zero. However, he showed that this maximum in fact depends upon the nature of the specimen, being significantly less for planes than for points, particularly when using objectives of relatively low NA. Both Sheppard (1989) and Wilson (1989) further showed that the axial resolution of a plane specimen is in fact significantly poorer in the case of confocal fluorescence than in the case of confocal reflection imaging, even when assuming the theoretical 'best case' in which the Stokes' shift is zero. This suggests that the use of colloidal gold rather than fluorescence labelling may be preferable in cases where optical sectioning is to be undertaken and the axial resolution of the specimen is to be maximised, particularly since the gold probes, unlike the fluorochromes, are not subject to photobleaching.

There are other definitions of depth of field that may be of greater practical importance in fluorescence microscopy. One of these is the variation of the *integrated* intensity of the image of such a point source, which is a measure of the total power in the image. This indicates how well the microscope discriminates against parts of the object not in the focal plane (Sheppard and Wilson, 1978*b*; Hamilton *et al.* 1981; Wilson and Carlini, 1988). In conventional microscopy, the integrated intensity of the light emanating from any one point in the specimen is unchanged as one moves a little away from focus, the light merely being redistributed in the final image, eventually contributing to a uniform background intensity that reduces specimen contrast (Born and Wolf, 1975; Wilson and Sheppard, 1984). This explains why the conventional optical microscope has no real resolving power in the direction of the optical axis. It is unable, for example, to provide any information as to the z position of a specimen consisting of a uniform layer of slightly absorbing or fluorescing material that lacks position-dependent structure in the plane normal to the optical axis, such as a solution of a fluorochrome held between a slide and a coverslip.

In contrast, the use of a circular imaging aperture during confocal imaging causes the integrated light intensity to fall off sharply as one moves out of focus, dropping to half the original value at a distance of 0.7λ from the focal plane along the optical (z) axis for a confocal transmission microscope with an objective of NA=1.0 and an ideally small confocal aperture (Sheppard and Wilson, 1978*b*; Wilson and Sheppard, 1984). In practice, this condition is rarely met, particularly for fluorescence imaging where the size of the imaging aperture is often increased to allow more light to reach the detector. Wilson and Carlini (1988), Wilson (1989), Sheppard (1989) and Brakenhoff *et al.* (1989) graph, for confocal reflection and confocal epi-fluorescence microscopy, the manner in which this degree of out-of-focus blur rejection diminishes as larger and larger confocal apertures are employed, and Wilson (1989) also describes the progressive loss of axial resolution that accompanies the use of fluorochromes with larger and larger Stokes' shifts.

It is thus clear that the optical sectioning performance of a confocal microscope depends crucially upon a variety of experimental variables: the nature of the specimen itself, the wavelength of the illuminating light, the Stokes' shift of the fluorochrome employed (in the case of fluorescence imaging), the numerical aperture and degree of aberration correction of the objective, and the size and shape of the confocal imaging aperture. One important conclusion is that significant rejection of out-of-focus information, flare and scattered light will be obtained both with circular imaging apertures significantly larger than required for true confocal imaging, and with slit apertures (Wilson and Carlini, 1988; Wilson, 1989). Another is that it is advantageous to have a confocal microscope equipped with a variable imaging confocal aperture, so that its size may be optimised for each particular application.

As a result of the improved z resolution discussed above, the vertical limits of a solution of a fluorochrome held between a slide and a coverslip, invisible in a conventional fluorescence microscope, may be clearly seen by CSFM, with an experimentally determined confocal resolution of the edge between the fluorescent solution and the overlying coverslip of 900 nm, obtained using a 1.25 NA objective at 514 nm excitation and 590 nm emission wavelengths (Wijnaendts van Resandt *et al.* 1985; Stelzer and Wijnaendts van Resandt, 1986). Brakenhoff *et al.* (1979, 1980) experimentally determined the axial resolution for a point object imaged in transmission mode to improve from 1.08 μm when imaged non-confocally to 0.75 μm when imaged confocally, using a 1.3 NA objective, light of 633 nm wavelength and circular confocal illuminating and imaging apertures, improving to about 600 nm when using blue (442 nm) light. In confocal fluorescence mode, with excitatory light of 488 nm and emission imaging above 520 nm, the single point axial resolution of their scanned stage SOM when imaging sub-resolution (90 nm) fluorescent beads was typically 730 nm (Brakenhoff *et al.* 1985, 1986).

Thus, by its intrinsic optical properties, the confocal scanning fluorescence microscope rejects out-of-focus blur at the outset, and produces raw images that, to a first approximation, contain only in-focus information. This can be appreciated by inspection of the confocal and non-confocal images of a tilted microcircuit, in which out-of-focus regions appear either dark (Fig. 3A) or blurred (Fig. 3B), respectively, and by comparing the unprocessed confocal images of fluorescently stained polytene chromosomes, collected independently using two different types of scanned beam confocal fluorescence microscope (Figs 4, 5) with conventional fluorescence micrographs of similar specimens after computational removal of out-of-focus blur (e.g. see Fig. 2B and 2D of Gruenbaum *et al.* 1984). A similar comparison may be made between confocal images of diploid anaphase *Crepis capillaris* chromosomes (Oud *et al.* 1989) with those obtained from the same material by computational deblurring of conventional fluorescence images (Rawlins and Shaw, 1988).

Lateral resolution enhancement

As with axial resolution, the use of an ideally small circular confocal imaging aperture, which causes the

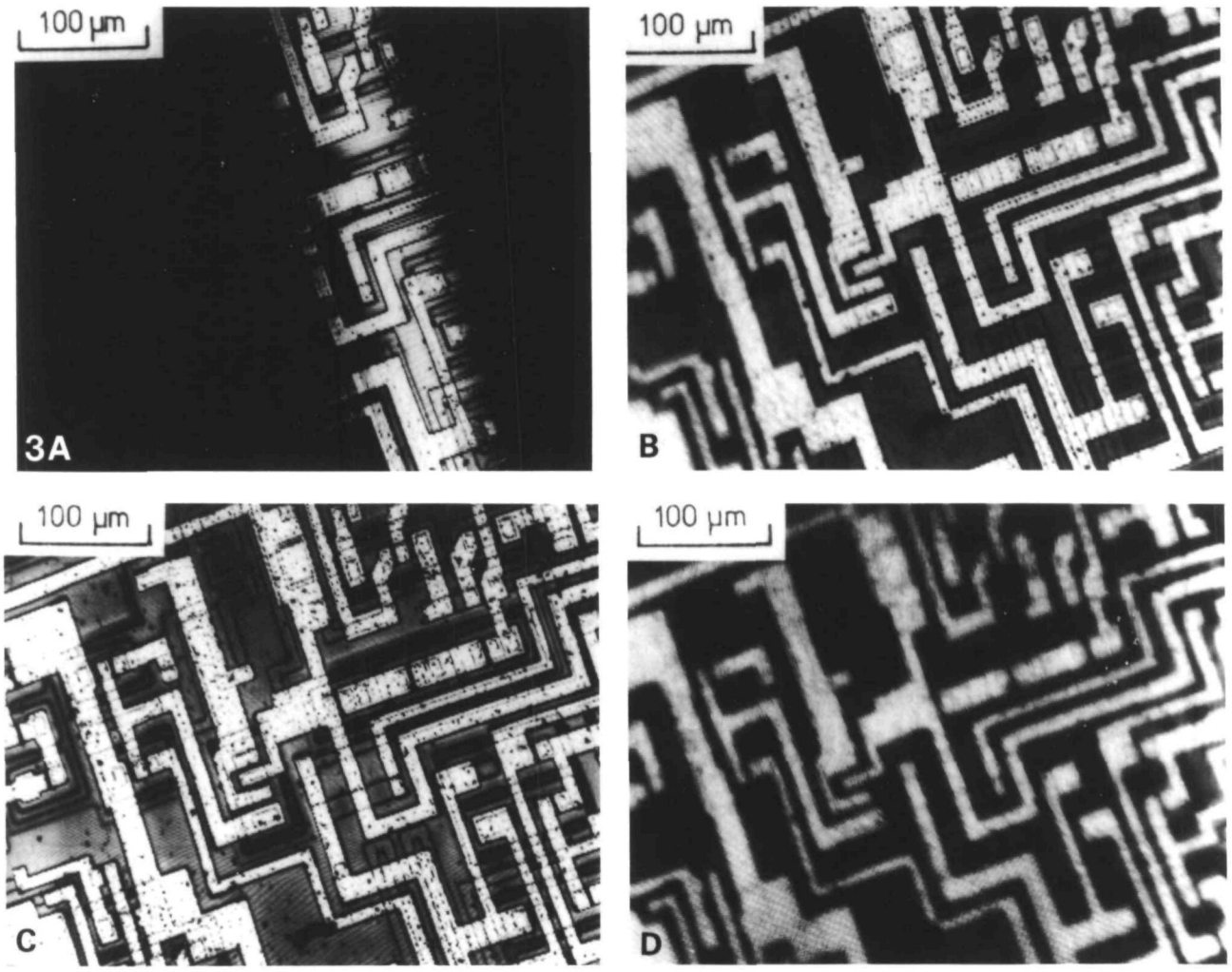

Fig. 3. A. A confocal SOM reflection contrast image of a tilted microcircuit, recorded with a 0.5 NA objective using light of 633 nm wavelength, in which only the central in-focus region is imaged strongly, the out-of-focus regions to the left and right, which lie above and below the focal plane, appearing dark. B. A non-confocal SOM reflection contrast image of the same specimen, in which the out-of-focus left and right regions of the specimen appear blurred. C. As A, a 20 μm axial z scan of the entire tilted microcircuit through the focal plane of the microscope having been performed during imaging using a piezoelectric z translator, resulting in the accumulation of an in-focus image of the entire specimen. D. As C, but with non-confocal optics, the axial scan having resulted in an entirely blurred image. Bar, 100 μm. Reproduced, with permission, from Wilson and Hamilton (1982).

PMT to function as a coherent point detector, results in an improved in-plane PSF for the confocal SOM, seen as a sharpening of the central peak of the Airy disc, with very weak outer rings, and gives a small but significant increase in lateral spatial resolution (*super-resolution*) over that achievable by conventional optical microscopy, by a factor of approximately 1.4 (Sheppard and Choudhury, 1977; Brakenhoff *et al.* 1979; Cox *et al.* 1982*a*; Wilson and Sheppard, 1984; Sheppard, 1987), the maximal theoretical confocal lateral resolution for light of 400 nm and a 1.4 NA objective being 130 nm (Carlsson and Åslund, 1987).

Together with the improved z resolution discussed above, this modest increase in lateral resolution obtained when using an appropriately small confocal aperture results in an in-focus sampled voxel that is about three times smaller in volume than when viewed non-confocally, significantly enhancing the optimal performance of the microscope (Brakenhoff *et al.* 1979, 1985, 1989). However, the detector must closely approximate an ideal point detector if true confocal operation, and the associated improvement in lateral resolution, are to be obtained. The ideally small confocal imaging aperture required to produce this super-resolution permits very little light to reach the photodetector, and thus may give a poor signal-to-noise level with weakly fluorescing specimens. In practice, therefore, apertures larger than that required for true confocal imaging are often employed. The effect of this on lateral resolution as well as out-of-focus blur rejection are discussed and exemplified in the recent important papers by Wilson and Carlini (1987*a*, 1988, 1989), Shuman (1988), van der Voort *et al.* (1988), Sheppard (1989) and Brakenhoff *et al.* (1989), and by Wilson (1989), who also shows how lateral resolution

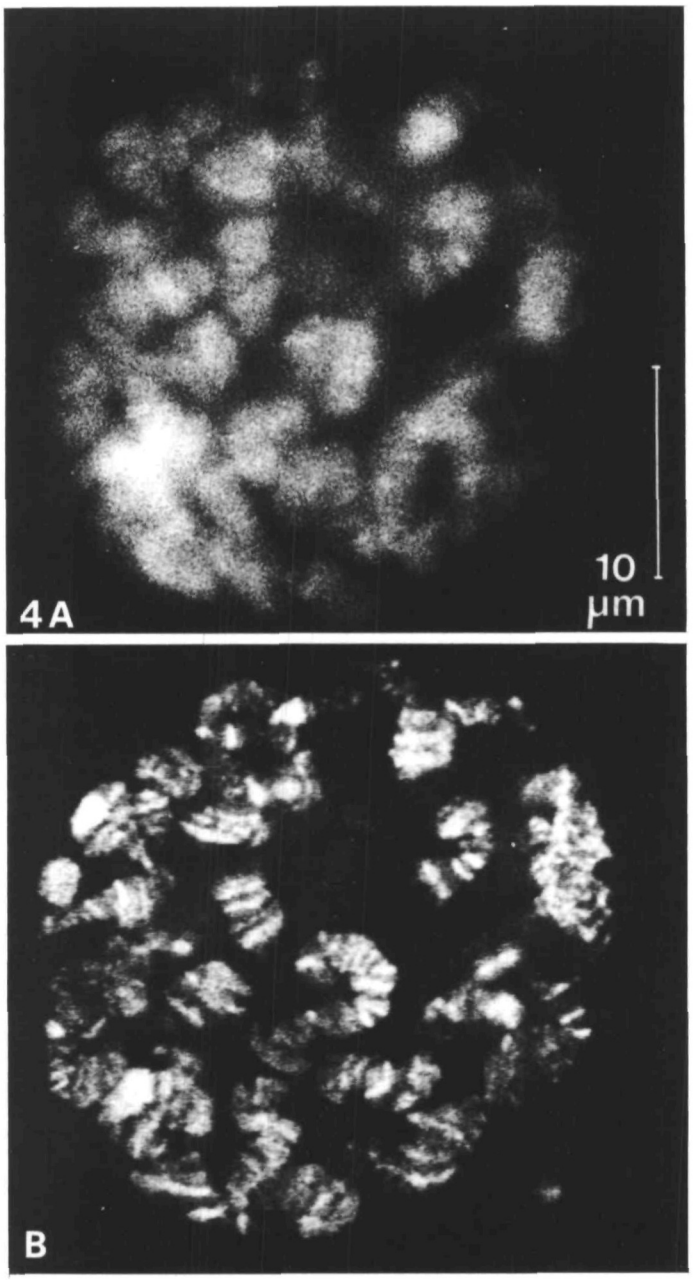

Fig. 4. An optical section taken through an intact but slightly flattened nucleus within a whole embedded salivary gland of a late third-instar *Drosophila melanogaster* larva, in which the DNA is stained with chromomycin A3, recorded on a prototype Bio-Rad Lasersharp MRC-500 scanning fluorescence microscope, using non-confocal (A) and confocal (B) optics. While the non-confocal image resembles conventional fluorescence microscope images of such specimens, the confocal image is free from out-of-focus blur, and comparable with the conventional fluorescence images after computational blur deconvolution (e.g. see Fig. 2 of Gruenbaum *et al.* 1984), revealing the fine banding patterns present on the large polytene chromosomes. Bar, 10 μm. Reproduced, with permission, from J. G. White *et al.* (1987).

decreases with fluorochromes of increasing Stokes' shift. If, in order to increase sensitivity when imaging faint fluorescent specimens, the imaging aperture is made larger than the diameter of the central maximum of the Airy disc, the benefit of increased lateral resolution is rapidly lost. In contrast, as discussed above, out-of-focus blur rejection is less sensitive to modest increases in confocal imaging aperture diameter, so that larger apertures may be used to obtain a high signal-to-noise ratio with reasonable optical sectioning, at the expense of loss of lateral super-resolution.

An even greater lateral resolution enhancement, by a factor of ×1.75, may be obtained if, with a circular illuminating aperture, the imaging aperture is made annular (Sheppard and Choudhury, 1977; Brakenhoff *et al.* 1979). However, this is at the expense of the improved z resolution obtainable with two circular apertures, discussed above, and leads to artifacts when imaging extended (i.e. three-dimensional) specimens (Brakenhoff, 1980). This modification is thus not desirable for biological confocal microscopy. More complex super-resolving apertures for confocal microscopy are discussed by Cox *et al.* (1982*b*) and Hegedus and Sarafis (1986).

As for axial resolution, these model calculations of lateral resolution have used the theoretical foundation laid by Born and Wolf (1975), based upon linear optics and a paraxial approximation that assumes relatively low numerical aperture, to calculate the PSFs of the lens(es). van der Voort and Brakenhoff (1989) have recently reported the development of a new theoretical model for confocal imaging based on electromagnetic theory, which takes proper account both of high NA lenses and the polarization state of the illuminating light (since laser illumination is inherently polarised). They show that the resolution obtained differs considerably according to the nature and orientation of the model specimen (points, horizontal lines, vertical lines, planes, etc.), fluorescently labelled membranes, for example, appearing brighter when oriented parallel to the optical axis, thus benefiting from the higher lateral spatial resolution, than when oriented perpendicular. They also point out that the confocal imaging of linear objects is strongly influenced by their orientation relative to the plane of polarization of the illumination, and recommend the use of circularly polarized light to circumvent this non-symmetrical response.

In practice, using a stage-scanning, high NA, single confocal imaging aperture system, Brakenhoff *et al.* (1979, 1980, 1985, 1986), by imaging sub-resolution (5–10 nm) holes in a gold film, measured the single point lateral resolution of their SOM (i.e. the width at half-height of the Airy disc image) to be 130 nm at λ=325 nm, 150 nm at λ=442 nm and 196 nm at λ=633 nm in confocal transmission brightfield mode with circular apertures, very slightly poorer than the theoretically expected values for their 1.3 NA objectives, and to be 220 nm in confocal epi-fluorescence mode, when imaging sub-resolution (90 nm) fluorescent beads, using excitatory light of 488 nm and fluorescence emission above 520 nm. More recently, using 50 nm diameter gold beads and a specially fabricated periodic fluorescent test specimen to enhance the signal-to-noise ratio by permitting signal averaging of weak fluorescence emissions, with 520 nm excitation and >580 nm emission wavelengths, and with a confocal

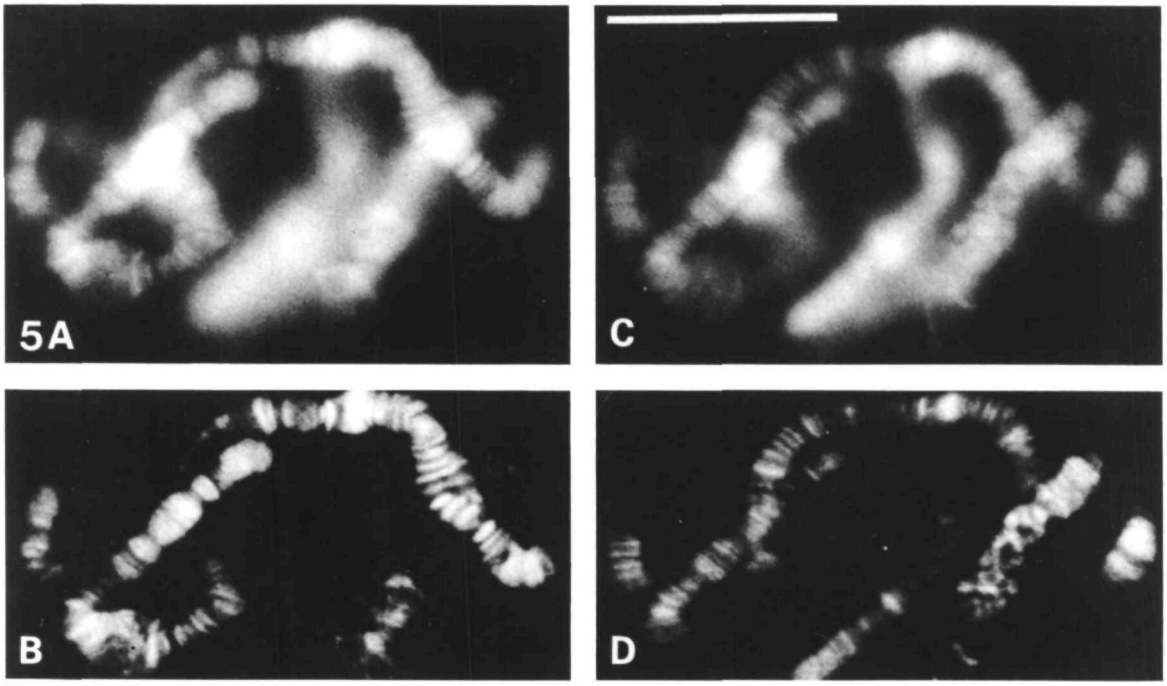

Fig. 5. Two optical sections at different focal planes separated by 4 μm of *Chironomus* polytene chromosomes, taken using a ×63/1.4 NA Planapo objective and 633 nm excitatory illumination on an experimental confocal version of the original Zeiss Laser Scan microscope, using non-confocal (A, C) and confocal (B, D) optics, showing features similar to those described for Fig. 4. Bar, 10 μm. Previously unpublished micrographs kindly provided by Dr A. Siegel of Carl Zeiss, Oberkochen.

pinhole that, when back-projected to the specimen plane, had a diameter of 400 nm, van der Voort *et al.* (1988) have refined these measurements, recording both lateral and axial resolution. They found the width at half-height of the lateral PSF to be 1.24 and 1.37 times greater than theoretical confocal value, for gold and fluorescence, respectively; the larger fluorescence value being in part due to the longer emission wavelength.

Carlsson and Åslund (1987) determined the in-focus resolution of their PHOIBOS SOM to be approximately 200 nm in confocal epi-fluorescence mode with an excitation wavelength of 458 nm and a NA 1.3 objective, using a confocal aperture diameter half that of the Airy disc, and W.B. Amos (personal communication) has shown the 270 nm spacings of the diatom *Amphipleura pellucida* to be easily resolvable by confocal reflection contrast microscopy (Fig. 6).

It is important to realise that high NA oil-immersion objectives are corrected for observation of specimens close beneath the coverslip. Thus when used for optical sectioning deep within aqueous specimens, their performance may become severely compromised by spherical aberration. It is much better to undertake serial optical sectioning of such specimens using a high NA water-immersion objective without a coverslip. Absence of chromatic aberration is also important for good confocal fluorescence imaging, particularly for off-axis imaging in scanned beam confocal systems, since its presence will cause a wavelength- and scan position-dependent axial shift in the optimal confocal position for the imaging aperture.

Confocal images, for all their advantages, are not perfect, and it should be possible to enhance them further by subsequent computational processing, as described for conventional fluorescence images by Agard (1984), Hiraoka *et al.* (1987) and Agard *et al.* (1989), to remove residual blurring due to the intrinsic limitations of the confocal optical system. In practice, this combination of optical and computational image enhancement has not yet been widely implemented, since the observed confocal images have in general been sufficiently clear to interpret directly.

Even greater super-resolution advantages have been explored theoretically by Pike *et al.* (1987), Bertero *et al.* (1987) and Sheppard (1988), achievable by imaging not just with a single on-axis confocal pinhole, but with an array of detectors which record both the on-axis and the off-axis light imaged from the illuminated voxel. The additional information obtained is processed by new algorithms for inverse problems based on the theory of singular systems, leading to a theoretical increase in lateral resolution to twice the Rayleigh criterion for coherent illumination, and of four times the Rayleigh criterion for incoherent illumination. While this approach is still in its formative stages, such a resolution enhancement has very recently been demonstrated experimentally for a low numerical aperture one-dimensional system by Young *et al.* (1989).

Discussion of resolution enhancement in scanning optical microscopy would not be complete without mention of a quite different method, near-field scanning optical microscopy (NSOM) (Lewis *et al.* 1984; Isaacson

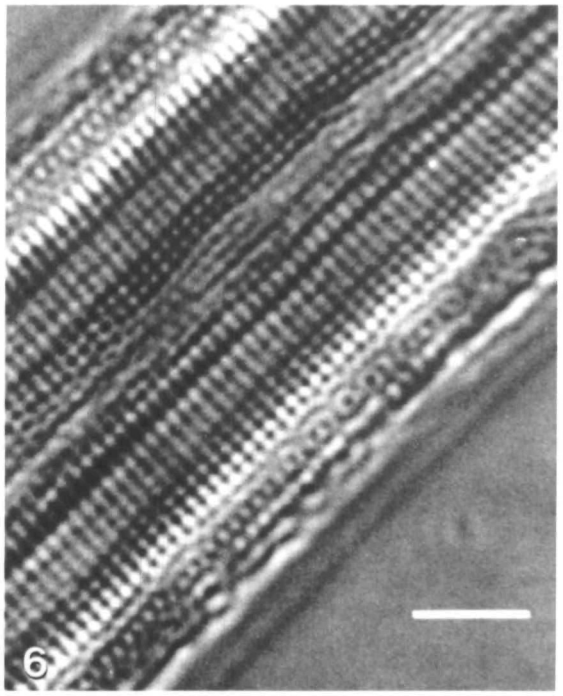

Fig. 6. Confocal reflection image of the shell of the diatom *Amphiplura pellucida*, showing the 270 nm spacing of the rows of dots, recorded using the Bio-Rad Lasersharp MRC-500 confocal scanning light microscope with a Nikon Planapo ×60/1.4 NA objective and 488 nm illuminating light. Bar, 2 μm. Previously unpublished photograph, kindly provided by W.B. Amos.

et al. 1986), a surface probing technique closely akin to scanning tunnelling microscopy (STM), that in principle can give spatial resolution of the order of one tenth of a wavelength. All the types of SOM discussed above are 'far-field' imaging techniques, limited by the constraints of Frauenhoffer diffraction. By contrast, NSOM produces images by illuminating the specimen with light emerging from a minute aperture in the tip of a highly tapered probe positioned in the 'near-field' region, at a distance of less than a wavelength from the specimen surface. At this proximity, the radiation emitted from the sub-wavelength diameter aperture has dimensions proportional to the size of that aperture and independent of wavelength. If the transmitted or fluorescently emitted light is then imaged onto a detector using conventional far-field optics, an image can be produced with enhanced spatial resolution. However, for this to occur the distance of the probe from the specimen surface must be kept constant; for example, at 20 nm±1 nm for a 50 nm diameter aperture used with 500 nm light, since the signal intensity varies exponentially with distance, as in STM. This is achieved by feedback control either of the tunnelling current or of the capacitance between the probe and the surface. Scanning the probe thus simultaneously generates both optical information (absorbance, fluorescence) and three-dimensional topographical information about the specimen surface, to a higher resolution than can be obtained by far-field CSOM. Its applicability to wet biological specimens has yet to be demonstrated, however, and its biological applications, as with STM, are more likely to be in the macromolecular domain.

Reduced image degradation due to light scattering and autofluorescence

In conventional transmission or epi-fluorescence microscopy, the entire observed area of the specimen is uniformly bathed in light (Fig. 1A). However, in SOM only one point in the focal plane of the specimen is illuminated with full intensity at any one time, illumination of other regions of the specimen being limited to a small cone above and below the in-focus voxel, in which the intensity is inversely proportional to the square of the distance from the focal plane (Fig. 1B). As a consequence of this, image degradation due to flare, light scattering or fluorescence emissions from other parts of the specimen is greatly reduced, even during non-confocal imaging (Cox and Sheppard, 1986; Wilson and Carlini, 1988). When imaging confocally, the additional rejection of light emanating from above and below the focal plane means that autofluorescence contributions from optical components and the immersion oil cease to be a problem. Thus the signal-to-noise ratio of the CSFM is significantly enhanced over a conventional fluorescence microscope.

Sensitivity, geometric linearity, dynamic range and photometric accuracy

Detailed quantitative studies of imaging sensitivity using CSFM are not yet available, although J. G. White *et al.* (1987) have estimated their prototype of the Bio-Rad Lasersharp MRC-500 instrument, operated in confocal fluorescence mode, to be about 2.4 times more sensitive than direct photography using high-speed film. Its absolute sensitivity is thus less than that of a SIT video camera, but since it has a lower dark current and gives less image background noise, it has an intrinsically higher signal-to-noise ratio. Thus, by using digital image averaging to reduce temporally varying noise, it can be used for the detection of weak signals.

A quantitative study reported by Ploem (1986, 1987) showed the PMT detection system of the original non-confocal Zeiss Laser Scan microscope to be capable of detecting approximately 10 fluorescein molecules per μm^2, a sensitivity some two orders of magnitude greater than conventional epi-fluorescence photomicrography using high-speed film.

In likeness with cooled CCD array cameras, scanned stage SOMs, and scanned beam SOMs that use linearly scanned scanning mirrors, do not suffer from the geometric image non-linearity characteristic of video cameras. Furthermore, the use of a PMT to measure the incoming light ensures a high dynamic range and good photometric accuracy. Thus CSFM images resemble CCD images in having intrinsically high data quality, although quantitative comparisons between the two image types have not yet been made.

Fluorescence photobleaching

In confocal microscopy, the instantaneous intensity of

the excitatory laser light at the in-focus voxel is considerably greater (about 250 000 times; White, J. G. *et al.* 1987) than that bathing the specimen in conventional epi-fluorescence microscopy using a mercury arc lamp (Fig. 1), if neutral density filters are not employed to attenuate the laser beam. Despite this, however, the total energy deposited in the specimen may be lower than during conventional full-field epi-fluorescence illumination (Baak *et al.* 1987), since only a tiny fraction of the total observed area of the specimen is illuminated at any one time (1/393 216th in an image of 768(H)×512(V) pixels, assuming equality between the area of a single pixel in the digital image and the cross-sectional area, a, of the diffraction-limited point of illuminating laser light at the focal plane). During scanning, irrespective of the scan rate, each part of the in-focus plane of the specimen is illuminated during only a fraction of the total time, $\Delta t = a/A$, where A is the total imaged area. (This is also assuming for simplicity that the scan rate is uniform over the entire field of view, which is not strictly the case in scanned stage SOMs using resonant scanning and in those scanned beam SOMs that use acousto–optic deflectors.)

J. G. White *et al.* (1987) reported that, using the prototype Lasersharp MRC-500 CSOM with its 25 mW argon ion laser attenuated to 2 mW intensity, which gave optimum results for fluorescein, the rate of fluorescein photobleaching was approximately half that of conventional epi-fluorescence microscopy using a mercury arc lamp. Bleaching of fluorescein was found to be greater for strongly stained features than for lightly stained ones, perhaps as a result of excitation saturation during the intense instantaneous illumination experienced during laser scanning, these strongly staining features thus decreasing in brightness disproportionately with time, leading to a progressive loss of contrast.

During laser scanning, regions of the specimen above and below the focal plane receive the same total flux as the in-focus voxel (ignoring absorption and edge effects), but at a lower instantaneous intensity and over a larger fraction of the total time, as is clear from Fig. 1B. Interestingly, J. G. White *et al.* (1987) found fluorescein photobleaching to be less in these less-intensely illuminated out-of-focus regions than at the focal plane. As in conventional fluorescence microscopy, anti-bleaching agents may be used to reduce the photobleaching problem, which might otherwise become serious during the collection of a complete set of serial optical sections.

Cremer and Cremer (1978) estimated the specimen temperature rise due to radiant heating within a single in-focus voxel during the short period of illumination by the scanned laser beam to be no more than 10^{-4} deg. C. Wilson and Sheppard (1984) gave a similar value. Thus, even if the assumptions underlying these calculations are out by several orders of magnitude, heating damage to the specimen during normal laser beam scanning is likely to be negligible.

One obvious application of confocal fluorescence microscopy that has yet to be realized is its use for fluorescence recovery after photobleaching (FRAP) experiments (Peters, 1985), in which the fluorochrome label in a particular area of the specimen is intentionally bleached by over-exposure to the illumination beam, and the rate of recovery of fluorescence intensity in this area is subsequently determined, in order to establish the translational diffusion coefficient or membrane permeability of the molecule to which the label is attached.

Further imaging modes using the confocal scanning optical microscope

Dual wavelength imaging

As in flow cytometry, it is possible, by the appropriate use of dichroic beam splitters and emission filters, and the addition of one or more additional photomultiplier tubes, to convert a single wavelength CSFM into a multiparameter instrument capable of simultaneously imaging two or more wavelengths. This has two major applications.

First, it enables the microscope to be used for the simultaneous visualization of at least two labels: for instance, colloidal gold particles, imaged at 488 nm by confocal reflection contrast, together with fluorescein emitting at a longer wavelength in response to excitation at 488 nm; or fluorescein and Texas red excited simultaneously by a multi-line argon ion laser.

Recently the first of a new generation of large Stokes' shift double fluorochrome conjugates, FR-1, has been developed by Molecular Probes, Inc. for use in single-wavelength excitation double-labelling applications. In this compound, a molecule of fluorescein is covalently linked to one of rhodamine. Like fluorescein itself, the conjugate can be excited at 488 nm, but, because of efficient energy transfer between the excited fluorescein moiety and the adjacent rhodamine, it fluoresces above 550 nm, enabling its emission to be easily separated from the 530 nm emission maximum of fluorescein, and thus imaged simultaneously (Haugland, 1987, 1988). Another new fluorochrome, Princeton Red, shares these spectral properties. The natural pigment phycoerythrin may also be excited at 488 nm and exhibits a large Stokes' shift. While widely used in flow cytometry, its rapid bleaching characteristics have so far limited its microscopic applications.

Photomultipliers are available with wide spectral ranges, capable of responding to wavelengths from 185 nm in the deep ultraviolet to 930 nm in the infrared, while tunable dye lasers can deliver excitation wavelengths across the whole visible spectrum from the near ultraviolet to the near infrared (van Geel *et al.* 1984; Williams *et al.* 1987). Thus with the appropriate choice of PMT, laser, filters and labels, the CSFM may be designed for multiparameter confocal fluorescence imaging over this whole range, as described by DeBiasio *et al.* (1987) for a conventional fluorescence microscope, but with the benefit of blur-free optical sectioning. The use of high-quality interference filters is necessary to ensure maximal separation of the fluorochrome signals, but since the emission spectra of many of the commonly used fluorochromes have long 'tails', this separation will never be perfect. Although this has not yet been implemented, it should be trivial to correct for any such

residual cross-talk between any two fluorescent channels electronically, as is done to separate the overlapping contributions of different isotopes during scintillation counting.

The second application of dual wavelength imaging, of enormous potential for the 3-D determination of physiological parameters within living cells, is the use of CSFM for direct simultaneous fluorescence emission ratio imaging (Tanasugarn *et al.* 1984; Tsien and Poenie, 1986; Bright *et al.* 1987). For this, one formerly required an ultraviolet laser, for use, for example, with Indo 1 to quantify intracellular free calcium concentrations (Grynkiewicz *et al.* 1985). However, several new physiological indicators have recently been developed for dual emission ratio imaging with excitation by an argon ion laser, including Flua-3 and Rhod-2 for calcium and the SNAFL and SNARF pH indicator series from Molecular Probes (Haugland, 1987, 1988), allowing this technique now to be applied using a standard dual-channel confocal microscope.

Alternatively, the CSOM may be equipped with an additional non-confocal detector for the scanned *transmitted* light. One elegantly simple method of achieving this is the use of a fibreoptic light guide that collects the transmitted laser light from below the microscope condenser and conducts it to be measured by the second channel PMT (Fine *et al.* 1988). If the host optical microscope has dark-field, phase-contrast or Nomarski DIC optical components, one may now simultaneously collect a conventional transmitted bright- or dark-field, phase-contrast or Nomarski scanned image and a confocal epi-fluorescence scanned image. Using an image processor, the distribution of the fluorescent label may then be displayed, either continuously or flashing, superimposed in a suitable pseudocolour upon the transmission image. *Confocal transmission* imaging (Brakenhoff *et al.* 1979, 1980) requires precise optical alignment of illuminating and imaging objectives and confocal apertures, and is not yet commercially available.

One great benefit of dual-channel imaging using a SOM is that the two images obtained are in exact spatial register, since corresponding pixels in each image are measured simultaneously during the illumination of a single voxel in the specimen. This greatly facilitates any subsequent image processing involving both images, such as the dual channel display or fluorescence ratio imaging discussed above, or the stereoscopic imaging and 3-D image reconstruction of a stack of optical sections, described below.

Other optical imaging modes, including differential phase-contrast

In addition to the straightforward confocal reflection contrast and epi-fluorescence SOM imaging modes, to the non-confocal scanned transmitted bright or dark-field, phase-contrast or Nomarski imaging made possible by combining the optical components of the host compound microscope with a confocal scanning attachment and a SOM detector for transmitted light, as discussed above, and to the various confocal transmission imaging modes requiring more complex optics discussed by Brakenhoff (1979), the SOM offers other imaging modes (Sheppard, 1987), those of phase-contrast (Wilson *et al.* 1985), transmission or reflection differential phase-contrast (DPC) (Sheppard, 1980; Hamilton and Sheppard, 1984; Wilson and Sheppard, 1984; Horikawa *et al.* 1987; Wilson, 1988), pure phase imaging obtained by integrating the DPC images (Hamilton and Wilson, 1984*a*), differential amplitude contrast imaging (Wilson and Hamilton, 1983), darkfield SOM (Wilson and Hamilton, 1985), polarization SOM for the study of birefringent objects (Wilson and Sheppard, 1985), optical-beam-induced contrast (OBIC) imaging of semiconductor devices (Wilson *et al.* 1986*b*), and confocal interference microscopy (Hamilton and Sheppard, 1982; Hamilton and Matthews, 1985), the potential of which for biological studies have yet to be fully explored.

The non-confocal DPC imaging mode is achieved by using a photodiode area detector split into two halves, in place of the PMT, the DPC image being generated by displaying the difference between the signals recorded from these semicircular detectors. Fig. 7 shows a critical-point dried but otherwise untreated fibroblast culture, viewed in air without an overlying coverslip by scanning reflection DPC microscopy, which resembles a conventional low-magnification transmitted Nomarski DIC image of such cells (White, N.S. *et al.* 1987), but with the advantages that it can be used on highly refractile specimens such as striated muscle, for which DIC is not always suitable, and for specimens on opaque or anisotropic transparent supports, such as plastic tissue culture dishes. Jeacocke (1989) has recently reported the successful modification of a dual-channel beam-scanning epi-illumination CSOM to provide *confocal reflection* DPC imaging, by substituting a half-aperture mirror in place of the conventional dichroic beam splitter, thus reflecting the left half-band to one confocal detector and the right half-band to the other, while Russ (1989) has obtained *confocal transmission* DPC imaging by reflecting the transmitted light, occluded for the left or right half-band at the back focal plane of the imaging objective, back through the optical path to a confocal epi-illumination detector.

Axial scanning, height profiling and vertical sectioning

The ability of the confocal SOM to record only in-focus information has two further advantages. First, it permits the instrument to be operated as though it had an infinite depth of field, rather than an extremely limited one (Wilson and Hamilton, 1982; Hamilton and Wilson, 1982*a*,*b*; Sheppard *et al.* 1983; Cox and Sheppard, 1983*a*; Wilson and Sheppard, 1984: Wilson, 1985*a*; Wilson *et al.* 1986*a*). By slowly and progressively changing the focal plane through the entire three-dimensional specimen (an axial z scan) while performing successive x,y scans, and by automatically accumulating only in-focus data into a single photographic or digital image throughout this process, a complete in-focus projection of the specimen down the z axis may be recorded, as a result of the confocal rejection of out-of-focus information (Fig. 3C). Additionally, since the position along the z-axis at which the maximum signal is recorded for a

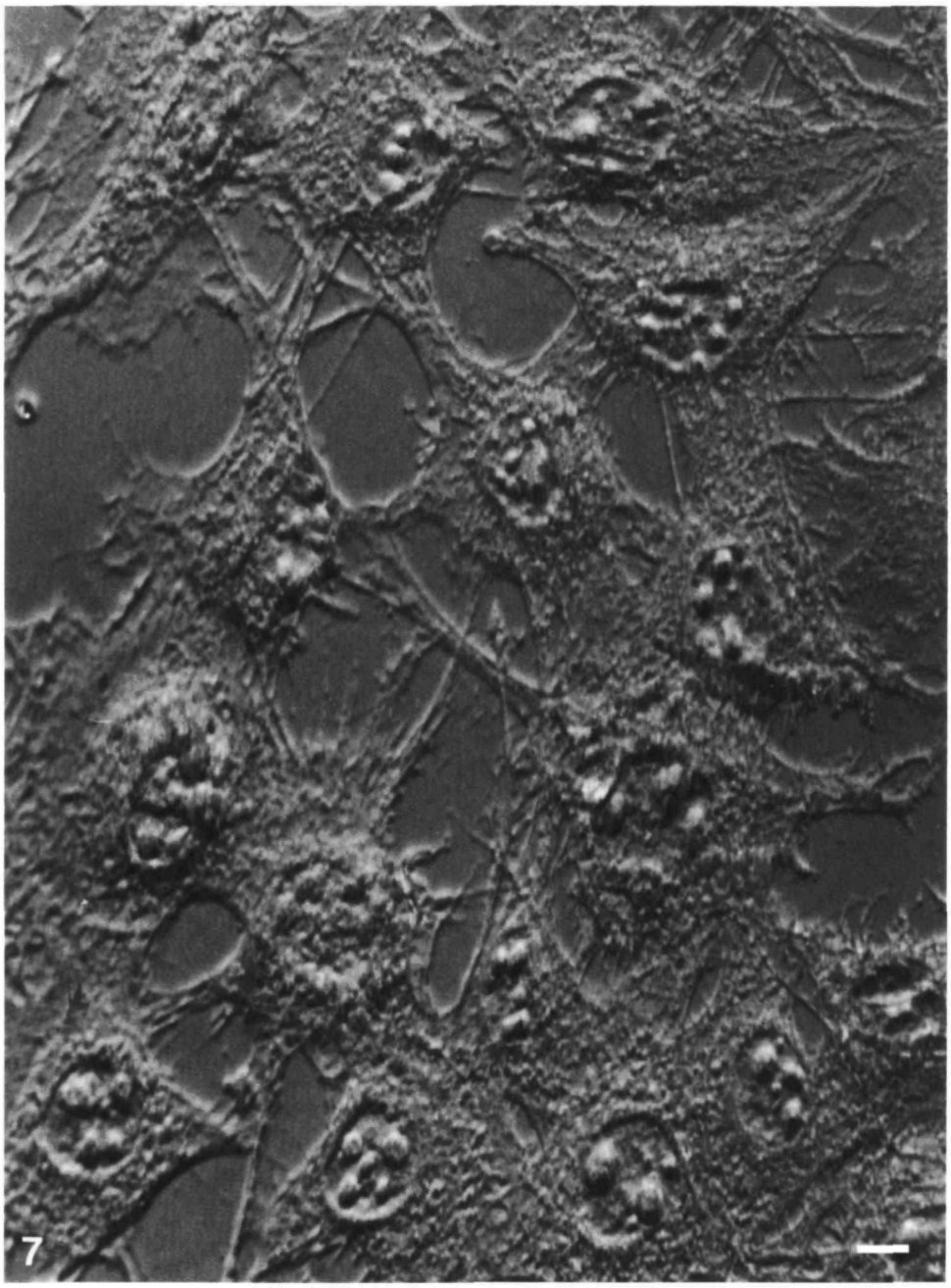

Fig. 7. A non-confocal reflection differential phase-contrast (DPC) SOM image of cultured mouse fibroblasts observed unmounted in air after critical-point drying. Stress fibres and larger cytoplasmic organelles are visualized within the cells, together with nuclei containing clearly defined nucleoli. This micrograph was obtained using a scanned-stage Lasersharp SOM-100 scanning optical microscope equipped with a 633 nm helium neon laser, a split photodiode detector (for DPC) and a Zeiss Epiplan ×40/0.6 NA dry objective with the correction collar set for a specimen without a cover-slip. Bar, 10 μm. Previously unpublished micrograph, described in N. S. White *et al.* (1987).

particular feature is by definition the in-focus position, axial scan data may be used to produce accurate height information of the specimen, which may be displayed either as a range image, in which lighter areas correspond to points closer to the observer, or as a 3-D height profile plot (Fig. 8). Height variations of the order of 0.1 μm have been clearly resolved by this method (Wilson and Sheppard, 1984). Further theoretical discussion and micrographs of non-biological specimens exemplifying these properties of the SOM have been presented by Sheppard (1982, 1987), Wilson and Hamilton (1984), Wilson and Sheppard (1984), Wilson (1985*a*), Wilson *et al.* (1986*b*) and Dixon and Martin (1986).

For biologists, one of the most novel and potentially useful imaging modes of the SOM is that of vertical sectioning (Wijnaendts van Resandt *et al.* 1985; Stelzer and Wijnaendts van Resandt, 1986). Instead of scanning in the x,y plane, it is quite feasible, while retaining all the advantages of confocal microscopy, to scan in x and z, thus generating images of optical sections *parallel* to the optical axis of the microscope. Thus transverse or longitudinal optical sections may be chosen of elongated structures (for instance, muscle fibres or embryos) lying on a microscope slide with their long axes oriented perpendicular to the microscope's optical axis, and both horizontal and vertical optical sections may be obtained from polarized epithelial cells cultured on a coverslip, as exemplified in Fig. 9. Scanning in z may be achieved by a motor drive on the microscope's focus knob, or by using a piezoelectric z translator between the microscope stage and the specimen (Wilson and Hamilton, 1982; Wilson and Carlini, 1988). In principle, by appropriately scan-

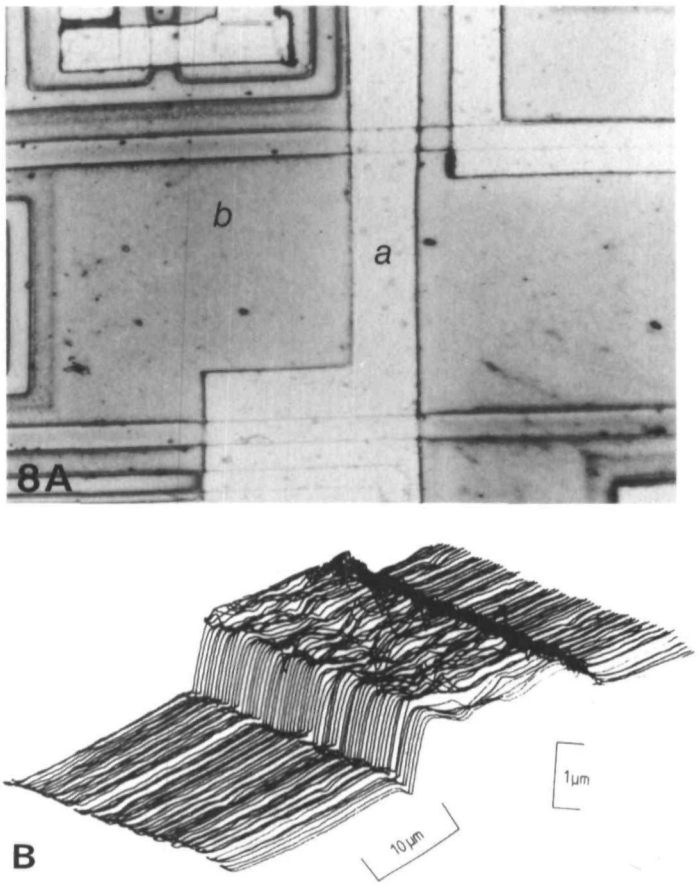

Fig. 8. A. A non-confocal reflection contrast SOM image of an area of a microcircuit, showing an evaporated metal strip (a) overlying the semiconductor (b). B. Height profile of a section of the metal strip on the semiconductor, determined from the in-focus maxima obtained by confocal axial scanning. Reproduced, with permission, from Wilson (1985).

ning x, y and z simultaneously, it would be possible to obtain oblique sections at any desired angle.

Reflection contrast imaging

As well as its usefulness for visualizing immunofluorescence, confocal SOM is capable, when used in a confocal reflection contrast mode, of generating interference reflection contrast images of focal adhesions in living cells on a glass coverslip (Gingell and Todd, 1979; Beck and Bereiter-Hahn, 1981; Verschueren, 1985; Amos *et al.* 1987), and of visualizing with high sensitivity the diaminobenzidine reaction product of immunoperoxidase labelling (Landegent *et al.* 1985; Baak *et al.* 1987; Cornelese-ten Velde *et al.* 1988) (Fig. 10). In principle, the confocal microscope should be superior to the conventional optical microscope for interference reflection microscopy, because of the confocal rejection of reflections from the upper cell surface. However, the published examples of such confocal applications are too few to evaluate.

Colloidal gold immunocytochemical labelling has revolutionised the electron-microscopic localization of known cellular macromolecules and organelles (reviewed by De Mey, 1983; Beesley, 1985), and De Brabander *et al.* (1985, 1986) and Geerts *et al.* (1987) have shown that conventional bright field and epi-polarization optics, in combination with video-enhanced contrast microscopy (reviewed by Shotton, 1988*a*) and suitable image processing and analysis, may be used to visualise, quantify and track individual sub-resolution colloidal gold particles in living specimens. This ability to coat gold particles with antibodies, cellular proteins or other ligands, and then to follow changes in their *individual* locations on or within living cells using the optical microscope, represents a revolutionary step towards a new cell biology, namely the study of dynamic macromolecular interactions within their natural environment, the living cytoplasm.

Gold beads of 5 nm can just be detected by confocal reflection SOM under optimal conditions (W.B. Amos, personal communication), as is also the case by video-enhanced contrast video microscopy (De Brabander *et al.* 1986). We have recently shown (White, N.S. *et al.* unpublished) that, when operated in a confocal reflection contrast mode using a ×63/1.4 NA oil-immersion objective, SOM gives clear images of sub-resolution 40 nm diameter gold particles, demonstrated to be individual gold particles rather than aggregates by electron-microscopic examination of the same fields. We have found the three-dimensional PSF of the confocal optics determined from serial optical sections of these gold particles to be considerably sharper than that obtained using sub-resolution fluorescent beads, in confirmation of the theoretical predictions of Sheppard (1989) and Wilson (1989). Furthermore, the absence of photobleaching has allowed us to collect *four*-dimensional data sets (i.e. to obtain a series of 3-D confocal images of serial optical sections at specified time-lapse intervals), and hence to study the

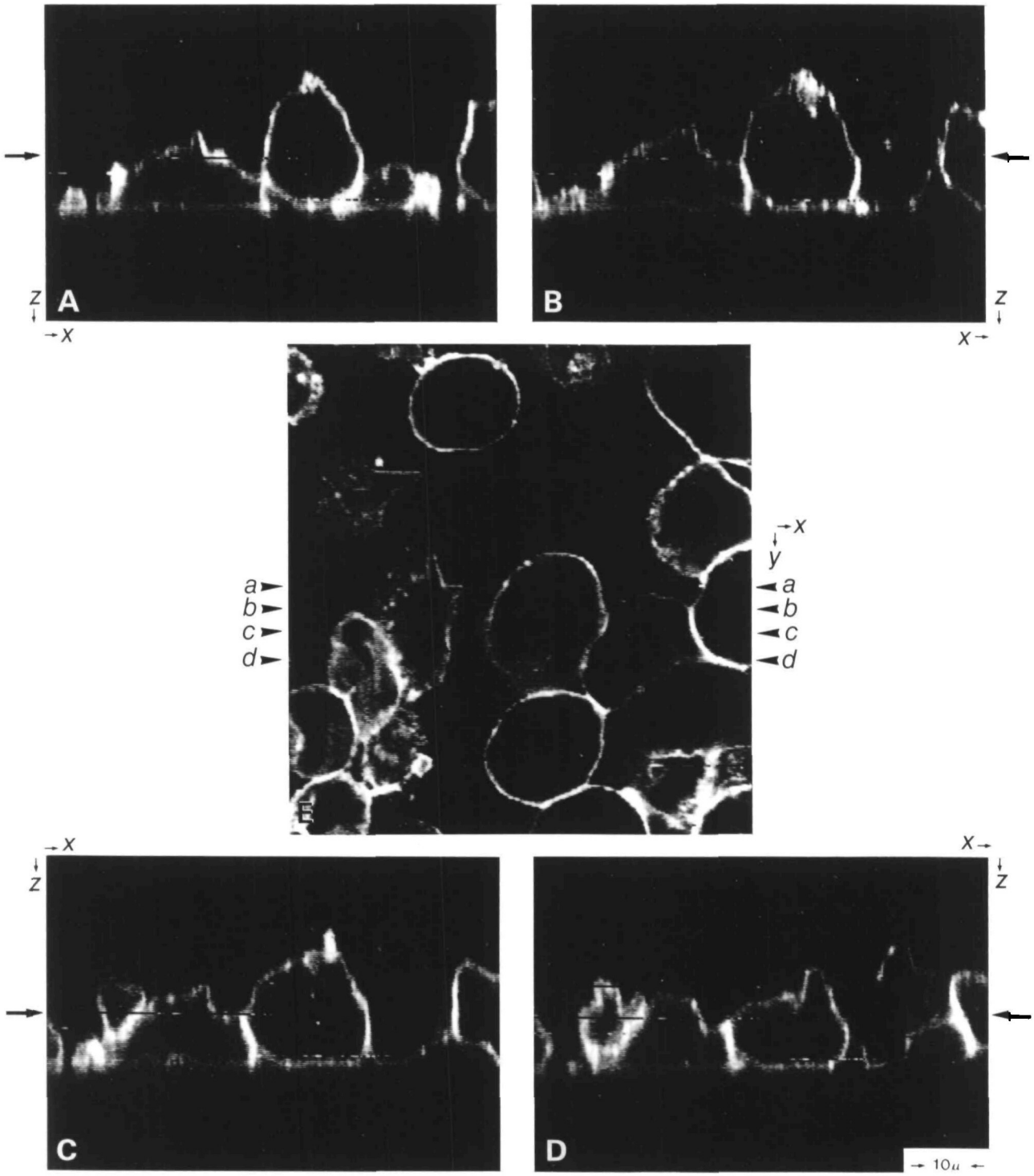

Fig. 9. A–D. A series of vertical (x,z) CSFM sections of cultured BHK (baby hamster kidney) cells labelled by fusion with liposomes containing *N*-rhodamine-phosphatidyl ethanolamine, made at the positions marked A–D on the control horizontal (x,y) CSFM section of the same cells shown in E. The arrows in A–D mark the focal plane (z axis position) at which the horizontal image, E, was recorded. For further details of the labelling procedure, see Fig. 15. Bar, 10 μm. Reproduced, with permission, from Stelzer and Wijnaendts van Resandt (1986).

redistribution of immunogold conjugates over the surface of living rat thymocytes during antibody-induced capping of surface antigens (White, N.S. *et al.* 1989). Fig. 11 displays selected optical sections and a stereoscopic projection of the complete 3-D data set showing the distribution of such immunogold labels on a partially capped cell.

Brakenhoff (1989) has pointed out that a potential artefact exists when imaging colloidal gold particles by confocal reflection contrast microscopy. If the particles

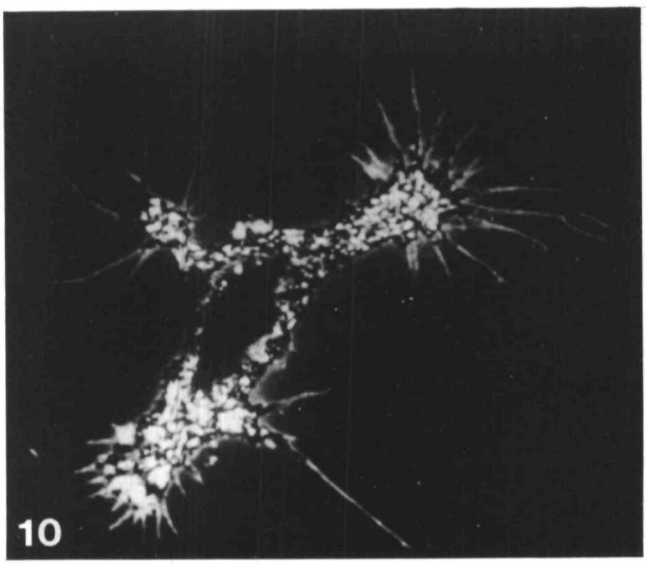

Fig. 10. Confocal reflection contrast image of a mouse peritoneal macrophage adhering to a coverslip, after staining of the surface antigens by the peroxidase method described by Cornelese-ten Velde *et al.* (1988). The fine filopodial extensions of the cell, which is about 20 μm in width, are clearly visible. Previously unpublished micrograph from the work of Cornelese-ten Velde *et al.* (1988), kindly provided by A. Dixon of Bio-Rad Lasersharp Ltd.

are separated by $\lambda/4$ along the optical axis, their coherent reflections along the optical axis will be exactly $\lambda/2$ out of phase and will suffer complete destructive interference, rendering both particles invisible. Whether this holds true in practice under high NA illumination, in which much of the reflected light is at oblique angles, remains to be investigated.

Biological applications of confocal scanning optical microscopy

Blur-free optical sectioning of single cells: applications in cell biology

Confocal scanning optical microscopy has only recently emerged from the realm of laboratory prototypes, employed to validate the technique itself, to become a reliable and important biological research procedure (White and Amos, 1987). However, to judge from the rapidly growing number of papers so far published on applications of this technique to current biological problems, it is clear that the confocal scanning optical microscope is capable of producing strikingly blur-free images, which give new understandings of biological structures and cellular processes.

Almost any fluorescently labelled specimen benefits from examination by CSFM, unless of course the narrow depth of field obtained is a distinct disadvantage. It is possible, for example, to clearly visualize and distinguish microtubules running above the nucleus of a cultured fibroblast from those that run around and below it (Fig. 12) (White, J.G. *et al.* 1987), to elucidate the otherwise invisible cisternal organization of the endoplasmic reticulum in spherical cultured plasmacytoma cells (Fig. 13) (Koch *et al.* 1987), and to distinguish individual spindle microtubules within an intact fertilised mitotic sea-urchin egg (Fig. 14) (White, J.G. *et al.* 1987). The technique has also been used with great elegance to study spindle rotations in living *Caenorhabditis elegans* embryos (Hyman and White, 1987), and to determine the 3-D chromosome arrangement in prophase and anaphase nuclei of *Crepis capillaris* (Oud *et al.* 1989).

The first biological applications of vertical (x,z) sectioning using CSFM have been those of Stelzer and Wijnaendts van Resandt (1986) and of E.H.K. Stelzer and G. van Meer (personal communication), who used it to observe the pH-induced fusion of fluorescently labelled liposomes with the apical surfaces of polarized virally infected MDCK cells. The subsequent freedom of the labelled lipids to diffuse into the basolateral membranes of these cells (Fig. 15) proves that tight junctions present no barrier to such diffusion. In a similar study, van Meer *et al.* (1987) employed the technique to demonstrate directly that lipids are vectorially transported from the Golgi to the apical and basolateral membranes of MDCK cells at different rates, under metabolic control.

Uses in cytology, cytometry and molecular biology

Munro and Pelham (1987) describe the use of CSFM to determine the cellular localization of a protein, grp78, normally restricted to the lumen of the endoplasmic reticulum, after transfection into COS cells with and without the C-terminal sequence that controls this localization. Because of the blur present in normal fluorescence images of the perinuclear region, its localization in the Golgi after removal of this sequence could only be checked confocally. The method has also been employed to study *in situ* hybridization, using fluorescent probes, to the centromeres of chromosome 1 in the nuclei of a human colonic adenocarcinoma cell line (P.M. Nederlof and H.J. Tanke, personal communication) (Fig. 16).

Baak *et al.* (1987) have used confocal reflection contrast microscopy to detect previously unobserved granula in Grimelius-stained sections of lung cancer, and to image proto-oncogene mRNA, detected by *in situ* hybridization with biotinylated probes complementary to c-*myc* oncogenes, at levels invisible by conventional optical microscopy.

Kalish *et al.* (1985) used the original non-confocal Zeiss Laser Scan scanned-beam SOM in a reflection DIC mode for the analysis of the band–interband pattern of spread air-dried polytene chromosomes from *Chironomus*, and Ploem (1986, 1987) has described its use with a low magnification (×2.5) non-immersion objective for the examination and measurement of fluorescence over large tissue areas (scanned area 3.75 mm×3.75 mm). He reports that its high contrast and sensitivity makes this an excellent instrument for the detection of very low concentrations of DNA-binding drugs in sections of brain and peripheral nerve, and that its low magnification makes it extremely easy to determine connectivity, for instance between neurones of a common neurotransmitter type

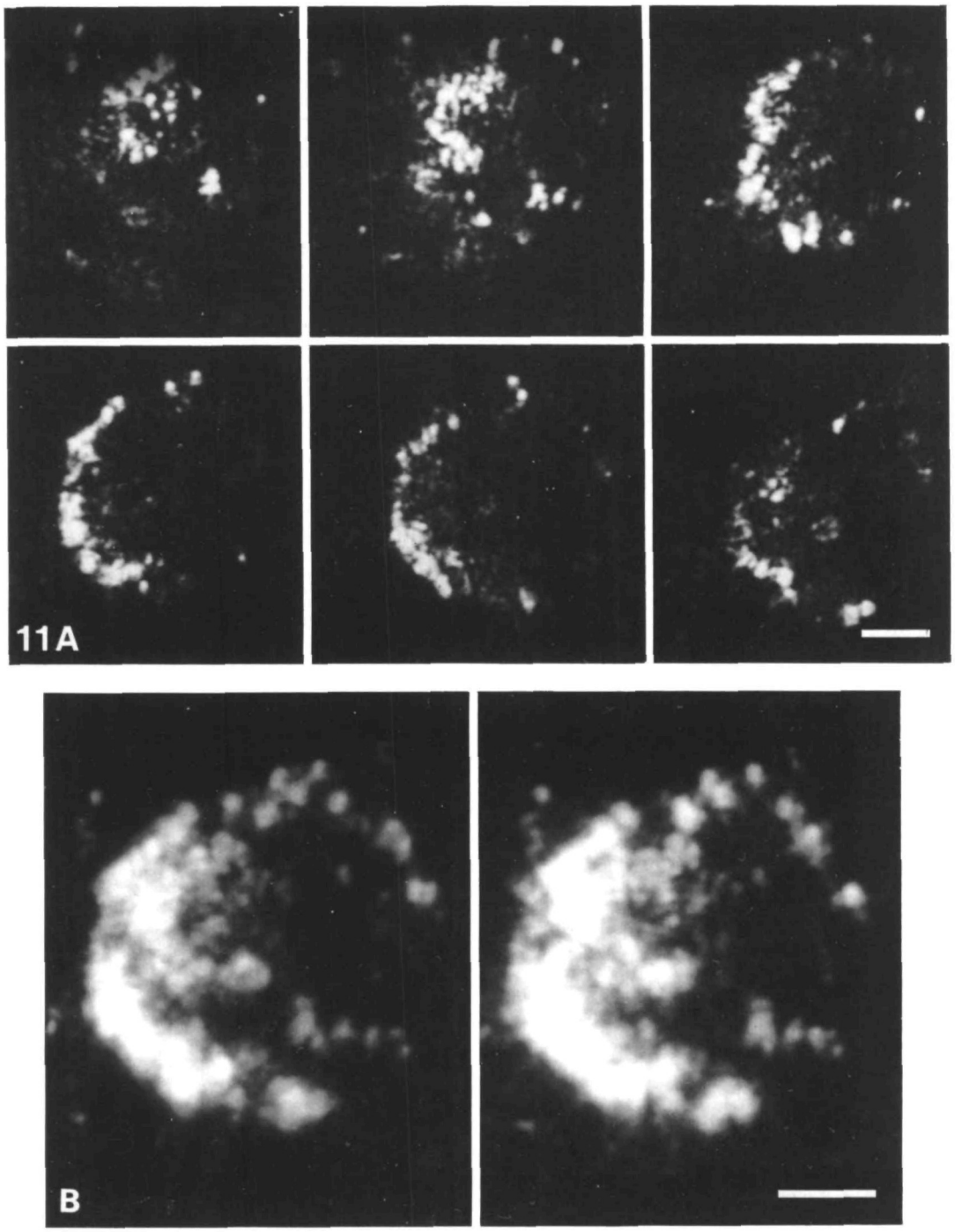

Fig. 11. Confocal reflection contrast images of a rat thymocyte labelled with a monoclonal antibody specific for the leucocyte sialoglycoprotein (LSGP), and partially capped by incubation at 37°C with a second layer of anti-mouse IgG conjugated to 40 nm colloidal gold particles, prior to fixation, clearing in Inhibisol and mounting in DPX. Gold particles giving bright reflections have accumulated over a relatively small area of the cell surface. A. Six optical sections selected at equal 800-nm intervals from the complete 3-D data set of 50 optical sections. B. A stereoscopic image pair (left eye image on the left) derived from the entire 3-D data set by projecting along axes inclined at ±6° to the optical axis and recording the average pixel intensity. Bars, 2 μm. Reproduced, with permission, from N. S. White *et al.* (unpublished).

labelled with a neurotransmitter-specific monoclonal antibody.

Although the application of confocal microscopy to automated cytometry has yet to be realised, Tucker (1987) discusses the use of non-confocal scanning cytometry for fast ploidy measurements and for abnormal cell location in cancer biopsies, and Bartels *et al.* (1987) are already developing a rule-based expert system, using

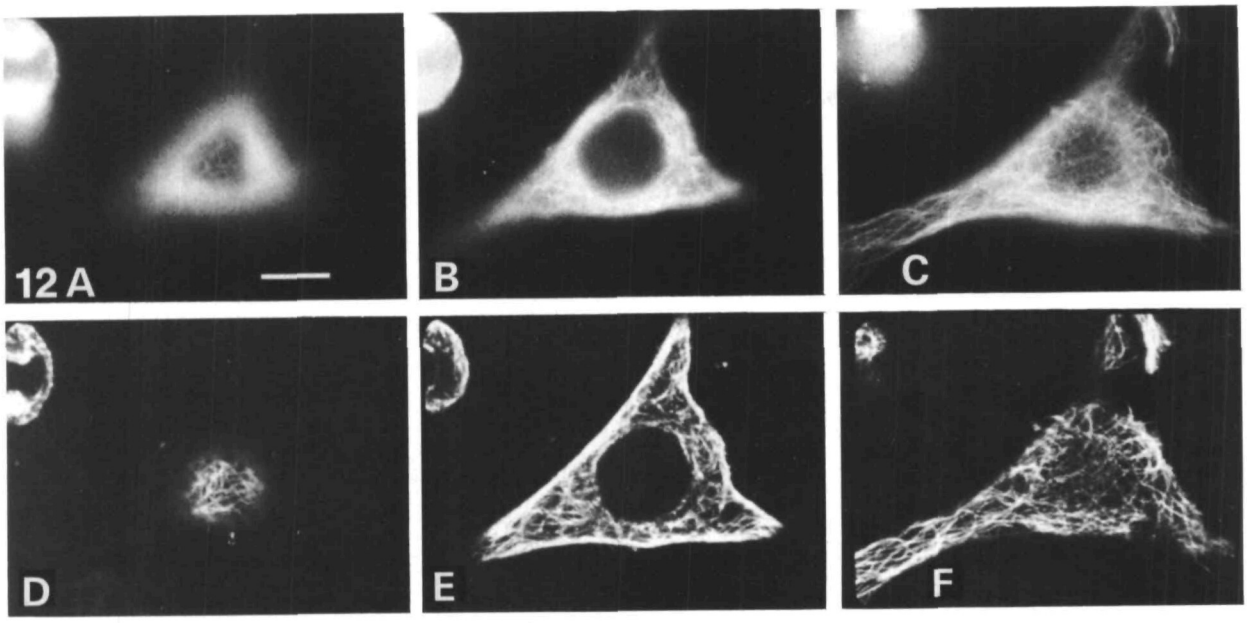

Fig. 12. A–C. Non-confocal; and D–F, confocal images recorded at three focal levels, near the top (A, D), the centre (B, E) and the bottom (C, F) of an unflattened HeLa cell stained with a monoclonal anti-tubulin antibody and with an FITC-labelled secondary antibody. The absence of out-of-focus blur in the confocal images is particularly noticeable in D and in the perinuclear region of E. Bar, 10 μm. Reproduced, with permission, from J. G. White *et al.* (1987).

parallel computer architecture to achieve sufficient speed, to permit the real-time image analysis of the data produced by their ultrafast SOM described above.

Applications in developmental biology, physiology, neurobiology and diagnostic pathology

Most studies using CSFM have employed high-magnification, high numerical aperture objectives, but since these have a limited working distance, they are not suitable for looking deep inside thick specimens. Carlsson and Åslund (1987) and Carlsson and Liljeborg (1989) have found ×40/1.0 NA objectives, which give working distances of 300–400 μm, to be a good compromise for studying the three-dimensional shapes of neurones, where the highest spatial resolution is not required. J. G. White *et al.* (1987) and White and Amos (1987), using much lower power objectives, have obtained good confocal fluorescence optical section images from labelled embryos, even when looking through half a millimetre or so of overlying fluorescently labelled tissue (Figs 17, 18). That such observations may be made non-invasively deep within suitably labelled unfixed or even living tissues has been shown for fresh mouse kidney (White and Amos, 1987; Fine *et al.* 1988), and is illustrated in Fig. 19, which shows neocortical neurones of an intact rat brain, the plasma membranes of which have been vitally stained by the voltage-sensitive styryl dye RH 414, and then viewed using the CSFM (Fine *et al.* 1988).

These few examples give every reason to believe that CSFM will find widespread applications in developmental biology, where it will permit the fates of individual microinjected cells to be followed and will allow the reorganization of vitally stained organelles to be observed during embryonic development; in physiology and neurobiology, for the non-invasive examination of living tissues, particularly using dual wavelength fluorescence ratio imaging to quantify physiologically important parameters such as intracellular pH, pCa and cell membrane potential; and in diagnostic pathology, where in particular it will make possible the rapid examination of biopsy specimens without the need to embed and section them.

Image processing of confocal image data sets

Three-dimensional cellular tomography

I have described how the confocal scanning fluorescence microscope may be used directly for non-invasive serial optical sectioning or opto-digital microtomy, to yield high-resolution images essentially free from out-of-focus blur. This permits direct three-dimensional cellular tomography, the acquisition and subsequent study of complete in-focus 3-D data sets (Brakenhoff *et al.* 1989).

Once a series of non-invasive optical sections has been collected by CSOM, the 3-D data set that these comprise may be manipulated in many ways, in common with similar data sets derived from deblurred conventional optical sections (Agard *et al.* 1989), and those obtained from X-ray or magnetic resonance tomographic imaging of the human body, or electron density maps of protein structures calculated from X-ray crystallographic analyses, to take two familiar non-microscopic examples. A great advantage of CSOM image sets is that they are already in spatial register, and thus do not require computational alignment before subsequent processing.

Because of the improved z resolution of the confocal image, such 3-D data sets should be more accurate representations of the fluorescence distribution in the original specimen than those obtained by the compu-

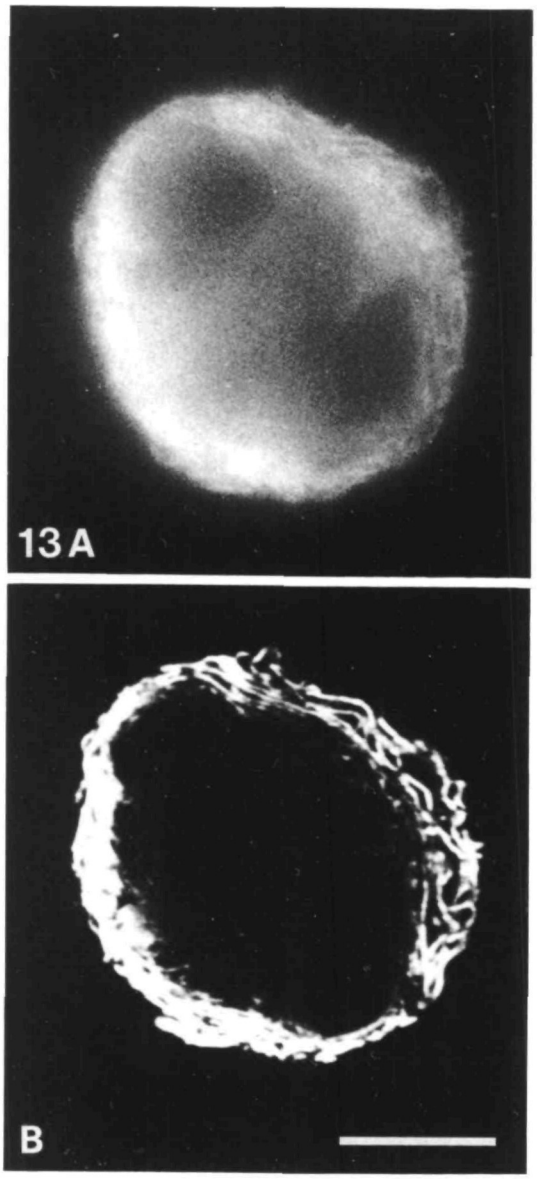

Fig. 13. A spherical plasmacytoma cell (line MOPC-315) stained with an antibody against endoplasmin, and imaged with the focal plane near the centre of the cell. The conventional image (A) is too blurred to be interpretable, while the confocal image (B) shows parallel concentric bright lines surrounding the unstained nucleus, which correspond to the individual cisternae of the endoplasmic reticulum seen in optical section. Bar, 10 μm. Reproduced, with permission, from Koch *et al.* (1987).

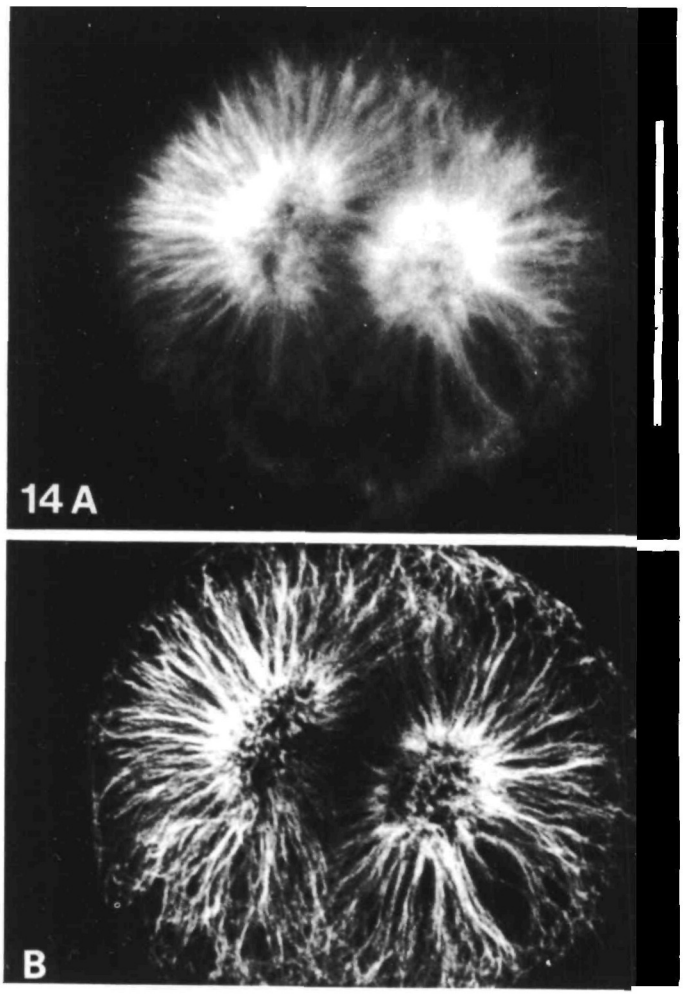

Fig. 14. A fertilized egg of the sea-urchin *Psammechinus* stained with anti-tubulin. A. Non-confocal; and B, confocal images, the latter showing with increased clarity the microtubules of the mitotic apparatus and at the cell periphery. Bar, 50 μm. Reproduced, with permission, from J. G. White *et al.* (1987).

tational deblurring of a set of conventional optical sections recorded at the same Δz intervals, provided that this interval is sufficiently small to avoid undersampling the z axis. Since the confocal spatial resolution along the z axis is intrinsically less than that of the lateral resolution, it has been found (van der Voort *et al.* 1989) that sampling in x and y every 100 nm, with an inter-section spacing of 400 nm, approximates well the Nyquist sampling theorem requirement for accurate digitization of a continuous image (Castleman, 1979), yielding elongated voxels of 100 (x) nm × 100 (y) nm × 400 (z) nm. Subsequent image processing, particularly stereoscopic display, must take account of the non-cubic nature of these voxels.

It should be noted that confocal x,z sectioning will not further increase this z resolution, unlike the procedure of rotating the specimen and resectioning to permit collection of the 'missing cone' data proposed by Agard (1984) and implemented by Shaw *et al.* (1989), which optimally brings the previously vertical z axis of the specimen into the horizontal plane in which the spatial resolution of the objective is maximal. Obviously such specimen rotation would also benefit the resolution of 3-D confocal images, but since the resolution along the z axis is initially greater, the effect would be less dramatic than with optical sections obtained by conventional fluorescence microscopy.

Stereology

The availability of high-resolution non-overlapping in-register optical section series makes it possible to undertake the accurate quantification of structural features in

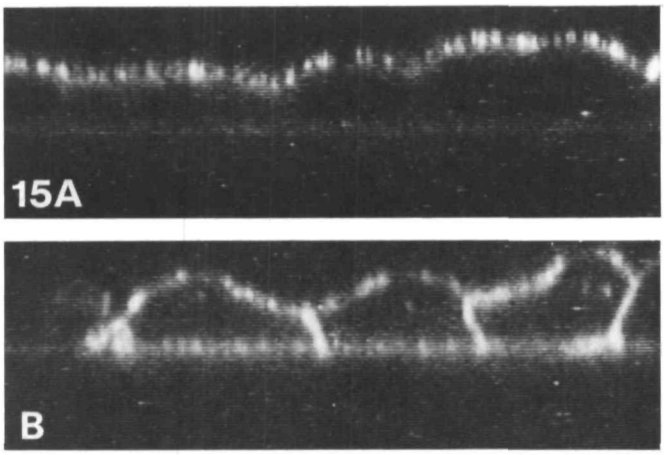

Fig. 15. Vertical (x,z) CSFM sections of a confluent culture of influenza virus-infected MDCK (Madin-Darby canine kidney) epithelial cells, each approx. 30 μm wide, growing on a glass coverslip, which have been exposed to liposomes containing *N*-rhodamine-phosphatidyl ethanolamine. A. When maintained at neutral pH, the apical surface only is outlined by adsorbed fluorescent liposomes. B. After incubation for 1 min at pH 5.0 and 37°C, during which viral glycoproteins on the apical plasma membrane induced fusion with the bound liposomes, the fluorescent lipid is found in both the apical and basolateral domains of the plasma membrane. Previously unpublished micrographs, kindly supplied by G. van Meer and E.H.K. Stelzer of the European Molecular Biology Laboratory, Heidelberg.

the specimen that has been thus sectioned, using the unbiased estimators for their three-dimensional stereological analysis described by Howard *et al.* (1985) and Cruz-Orive (1987).

Stereoscopic imaging

One of the most straightforward and useful image manipulations that may be applied to such a data set is the generation of stereoscopic pairs of images, permitting the results to be directly inspected in three dimensions. As with a conventional optical microscope (Osborn *et al.* 1978), stereo pairs in confocal microscopy may be recorded directly from the microscope, by occluding first the left and then the right halves of the back focal plane of the imaging objective, thereby selecting only the right and left side-bands of the image transform, respectively, but with the advantage that this may be done without the impairment in spatial resolution consequent upon conventional stereoscopic imaging (Sheppard and Hamilton, 1983). However, it is more usual to collect a complete series of confocal optical sections, and to generate the stereo pairs, either 'on the fly' (Inoué *et al.* 1985; Inoué and Inoué, 1986) or subsequently, by the mathematical projection of the complete 3-D data set down two selected axes corresponding to the required left and right eye views. This may be achieved by combining all the sections, pixel by pixel, after small incremental shifts of successive sections by a constant displacement to right or left. For shifts involving integral numbers of pixels, this is straightforward and rapid to achieve using a simple image processor, enabling rapid stereoscopic display, as described by Cox and Sheppard (1983*b*), Brakenhoff *et al.* (1985), Inoué *et al.* (1985), Inoué and Inoué (1986), Takamatsu and Fujika (1988) and van der Voort *et al.* (1989), although this method places restrictions on the possible stereo angles obtainable between the left and right eye images. Complete flexibility, at the expense of speed, may be obtained by non-integral shifts involving pixel grey-level interpolation (Brakenhoff *et al.* 1985; Carlsson and Åslund, 1987), achievable in software or by use of a sophisticated image processor.

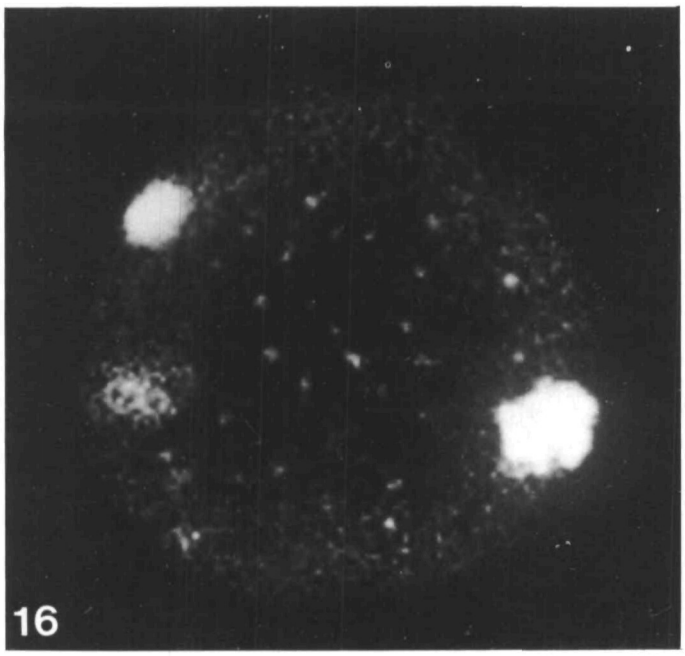

Fig. 16. A confocal optical section through the intact nucleus of a cultured 5583-E human colonic adenocarcinoma cell in which the centromeres of chromosome 1 have been stained with a biotinylated DNA probe and fluorescein–avidin, using the procedures given by Nederlof *et al.* (1989). This cell line contains three copies of chromosome 1. The centromeres of two of these lie in the focal plane, while the third lies just below it, thus appearing with weaker intensity. The cause of fluorescent labelling at the numerous smaller loci, previously unseen by conventional epi-fluorescence microscopy, has yet to be established. Previously unpublished micrograph from the work of P.M. Nederlof and H.J. Tanke, kindly provided by A. Dixon of Bio-Rad Lasersharp Ltd.

Surprisingly few sections (as few as 12) are required to generate a stereoscopic image in which the individual planes are not perceivable (Takamatsu and Fujika, 1988; van der Voort *et al.* 1989), and inclusion of all the sections from a large serial-section data set may indeed result in confusing stereoscopic images, because of superposition of detail at different depths. This reflects the fact that the human eye is less sensitive to variations in stereoscopic

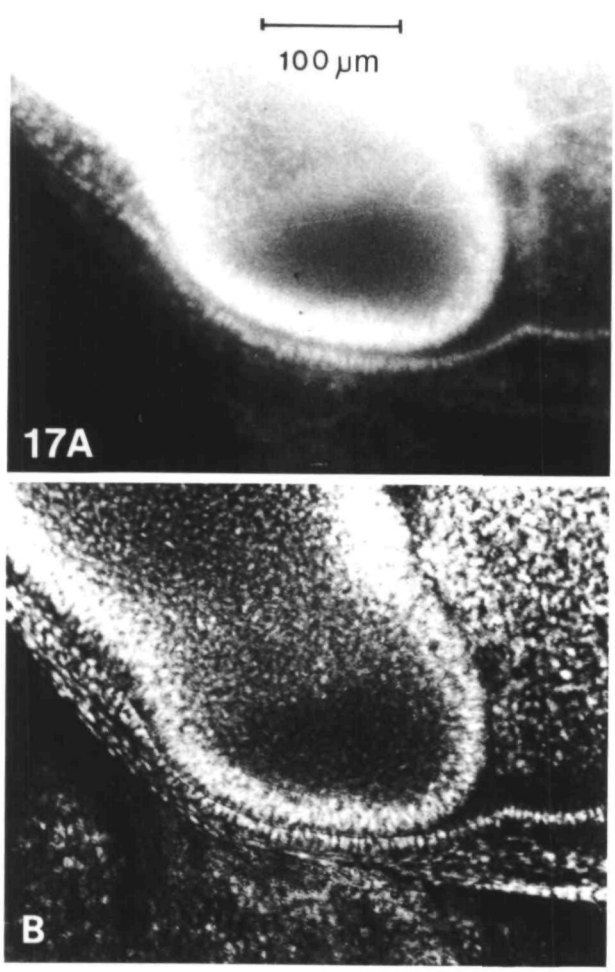

Fig. 17. A. Conventional; and B, confocal optical section images through part of the head of an intact chick embryo at the 12-somite stage, imaged with a ×6.3/0.2 NA objective at a depth of 0.5 mm within the fluorescently stained tissue. The numerous bright bodies are nuclei stained with the DNA-specific fluorochrome chromomycin A3. The confocal image shows details of the optic vesicle, lens ectoderm and amnion with much greater clarity than does the non-confocal image. Bar, 100 μm. Reproduced, with permission, from J. G. White *et al.* (1987).

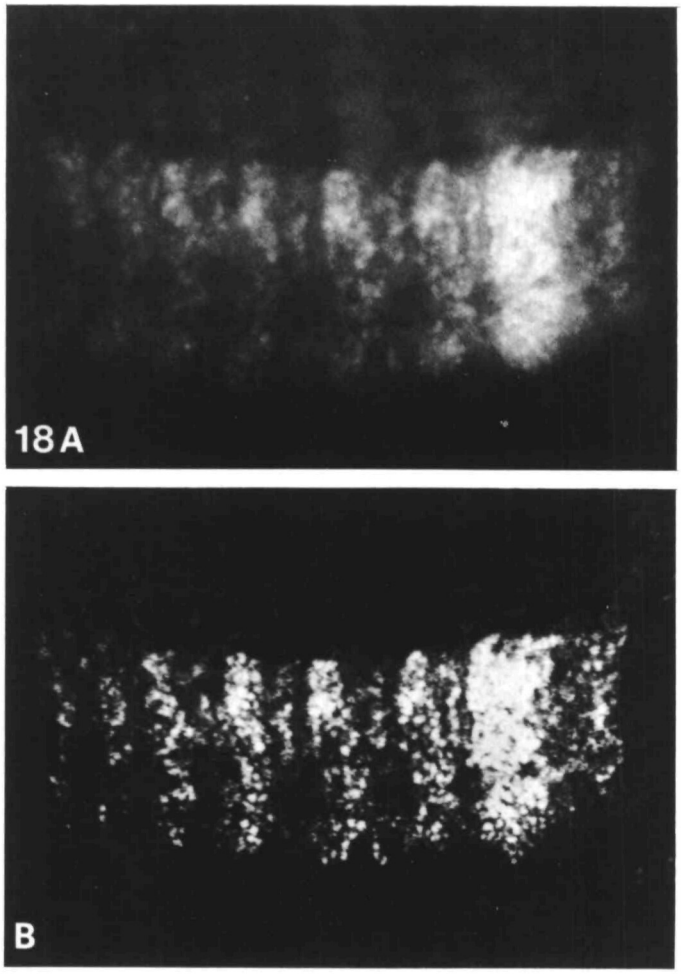

Fig. 18. A. Conventional; and B, confocal optical section images through a segmented *Drosophila* embryo stained with a fluorescein-labelled antibody to the *bithorax* gene product. The numerous bright bodies are the nuclei of individual cells within the developing nervous system. The intersegment spacing is approx. 70 μm. Reproduced, with permission, from White and Amos (1987).

depth than in lateral directions. Furthermore, a significant fraction of the population (about 10 %) are unable to perceive depth from such stereoscopic pairs, a condition that may be related to the amount of visual stimulation received in early infancy.

Such stereo image pairs may be viewed stereoscopically in a number of ways designed to ensure that the right image is not seen by the left eye and *vice versa*, the most common of which, in order of increasing sophistication (and cost!), are as follows. The images may be displayed: (1) as side-by-side photographic prints or images on a single video monitor, requiring parallel or cross-eyed stereoscopic fusion, either by 'free-viewing' or by using a simple optical aid incorporating lenses and/or mirrors; (2) as a red/green anaglyph photograph or image on a colour monitor viewed through red/green spectacles; (3) as separate images on two monitors fitted with polarizing screens of opposite polarity, viewed superimposed by means of a half-silvered mirror while wearing appropriately polarizing spectacles (one image being laterally inverted by reversing the polarity of the horizontal scan driver on one of the monitors); (4) as full-screen video images occupying alternate video fields on a single monitor, viewed either through PLZT or liquid crystal shutter spectacles, in which the left and right shutters are alternately made opaque in synchrony with the video field display frequency, or through circularly polarizing spectacles and a liquid crystal screen fitted to the monitor, which switches the state of circular polarization of the viewed image from clockwise to anti-clockwise and back again in synchrony with the change in displayed image; or (5) as full-screen superimposed colour video images projected from two aligned videoprojectors through left and right polarizing filters onto a non-depolarizing screen, viewed using polarizing spectacles.

The manner in which the individual sections should be

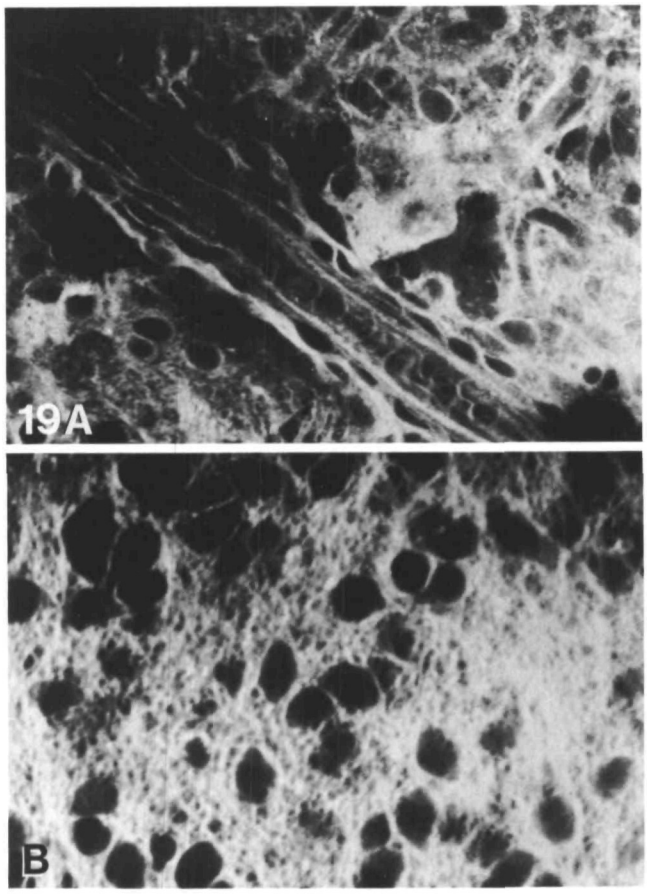

Fig. 19. Confocal images of neocortical neurones of an intact rat brain. After craniotomy and reflection of the dura, the fluorescent voltage-sensitive styryl dye RH 414 was added for 30 min to the artificial CSF bathing the exposed cortex, and was then washed off before viewing. A. Cells close to the pial surface can be seen adjacent to an erythrocyte-filled capillary. Cell bodies appear dark, surrounded by the brightly fluorescent, stained cell plasma membranes and processes within the neuropil. B. Cell bodies and processes imaged at least 250 μm below the pial surface. Note that the overlying blood vessel seen in A is completely invisible at this plane of focus. Reproduced, with permission, from Fine *et al.* (1988).

combined for this purpose is to some extent a matter for subjective evaluation, depending upon the nature of the specimen being imaged. The simplest procedures are merely to average the pixels in each projected column, or alternatively to record the value of the brightest pixel, a procedure that works surprisingly well for many specimens, despite its inability to remove hidden lines and surfaces (van der Voort *et al.* 1985, 1989). However, more convincing images may sometimes be obtained by exponentially weighting and then averaging or summing successive sections (Carlsson *et al.* 1985; Inoué *et al.* 1985; Inoué and Inoué, 1986), in such a way that the front of the specimen is made to appear brighter than the rear, or as a different pseudocolour (Boyde, 1987), thereby adding an extra depth cue to that of parallax. Such 'weighting' may also be made during data collection, by collecting the front sections first, and allowing photobleaching to reduce sequentially the intensity of rearward sections! Alternatively, if the *front-most* voxel exceeding a given threshold is selected, a surface image is obtained. Fig. 20 exemplifies the usefulness of the stereoscopic approach for visualising chromosomes imaged by confocal fluorescence microscopy in a mitotic diploid neuroblastoma 2A cell (Brakenhoff *et al.* 1985).

Schormann *et al.* (1989) have observed that, when a large number of optical sections and too-extensive lateral shifts are employed during stereo pair generation, the stereo images show low contrast and poor depth effect, attributable to suppression of contrast of structures with orientations orthogonal to the direction of shifting. They have consequently explored image-processing procedures to improve the clarity of confocal stereo pairs by enhancing the contrast and edges of the individual images before their use in stereo pair generation. They have found that the use of a modified Wallis transformation, which amplifies the contrast of very subtle structures by calculating local means and variances, either alone or in combination with a Sobel edge enhancement operation, results in a remarkable sharpening of stereo pair images generated from sets of either Nomarski or confocal fluorescence optical sections. Carlsson and Liljeborg (1989) have similarly used a 3-D gradient filter to emphasize edge information, while Sheppard and Cog-

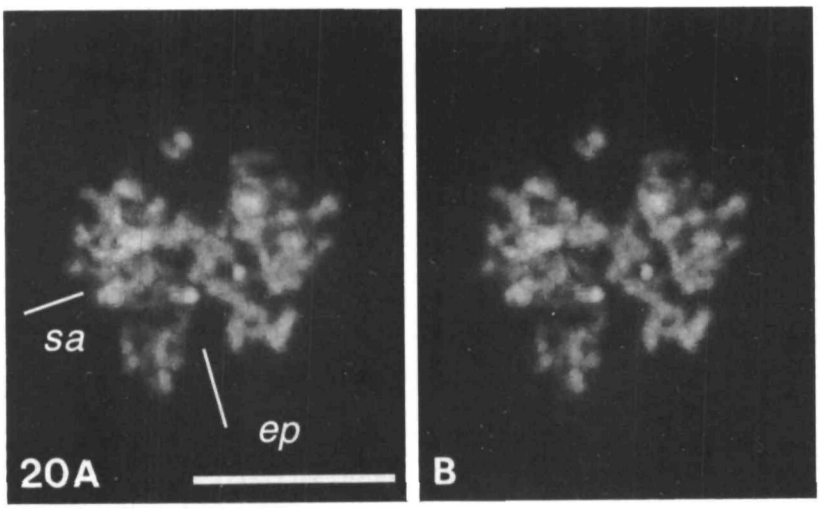

Fig. 20. A pair of stereo micrographs, prepared as described in the text by recording the maximum pixel value of a set of confocal optical sections when projected, after slight incremental left or right transverse shifts, onto a horizontal plane surface. The specimen is an early anaphase mouse neuroblastoma 2A nucleus, in which the DNA has been stained with mithramycin. The orientations of the spindle axis (sa) and the equatorial plane (ep) are indicated, and the individual chromosomes can be clearly seen, separated from one another within the spherical space occupied by the entire nucleus. Bar, 10 μm. Reproduced, with permission, from Brakenhoff *et al.* (1985).

giswell (1989) have suggested the subtraction of 0.5 times the pixel values of a low spatial resolution confocal image, acquired using a large confocal imaging aperture, from those of a high resolution one, obtained using a small aperture, as a form of 'unsharp masking' for edge enhancement. van der Voort *et al.* (1985) previously developed another algorithm for local contrast enhancement, which they used to match better the high dynamic range of single CSFM images to the more limited dynamic range of most display systems. This stretches the contrast of dark areas of the image, or of both dark and light areas, but acts to preserve edges in local areas in which both dark and light pixels coexist. van der Voort *et al.* (1989) described extensions of several of the common two-dimensional image-processing algorithms, including the Sobel filter, to work directly on three-dimensional CSOM data sets.

Simulated fluorescence emission

An alternative non-stereoscopic image display mode for a three-dimensional CSFM data set, particularly useful for compact fluorescent objects, is that of displaying them as if surface shadowed or surface luminant. van der Voort *et al.* (1989) have developed a very effective algorithm for

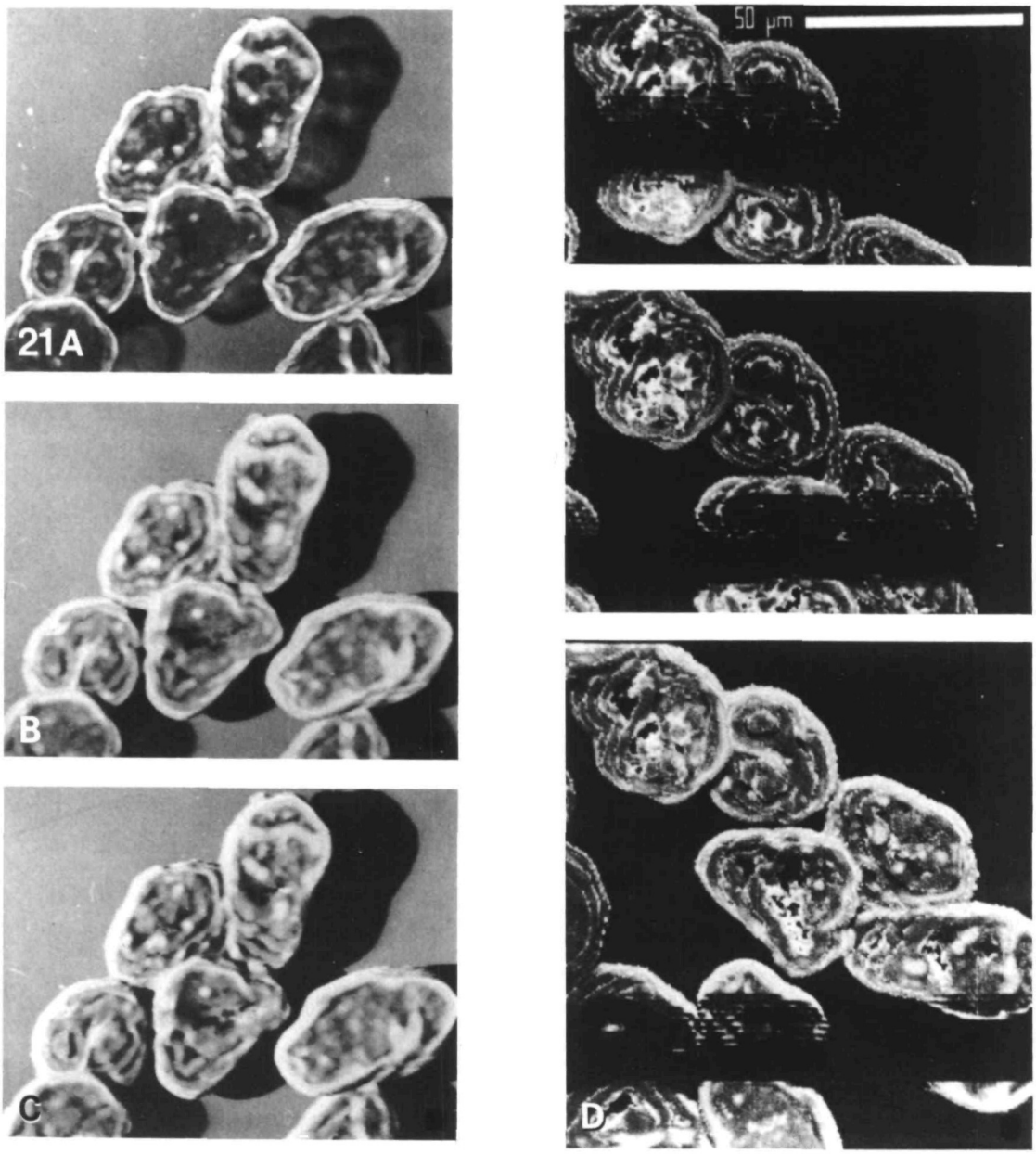

Fig. 21. Simulated fluorescence emission process images of the nuclear lamina of an embryo carcinoma cell line (P19EC). Twelve original confocal fluorescence optical sections have been used, and a homogeneous background has been added to allow the formation of artificial shadows. A–C. Using different degrees of object transparency. D. Demonstrating the ability to use an 'electronic knife' to section the three-dimensional objects artificially in a plane orthogonal to that of the optical sections, thereby exposing the internal structure of the specimen. Bar, 50 µm. Reproduced, with permission, from van der Voort *et al.* (1989).

Table 1. *Advantages and disadvantages of unitary beam confocal laser scanning microscopy*

Confocal

Advantages

1. Permits rapid, easy, non-invasive serial optical sectioning deep within intact, or even living, three-dimensional specimens
2. Optical rejection of out-of-focus information, reducing or obviating the need for subsequent computational deblurring by yielding raw images that are essentially blur-free
3. Reduced light scattering and autofluorescence
4. Significantly increased axial (z) resolution over conventional optical microscopy
5. Possibility of extended depth of field and height profiling by axial scanning
6. Improved lateral (x,y) resolution, if the confocal aperture is sufficiently small
7. Lack of image registration problems between dual channel images and in 3-D data sets, facilitating subsequent image processing and generation of stereoscopic images

Disadvantages

8. Use of a small confocal aperture reduces overall image intensity
9. Out-of-focus structures invisible (However, conventional optics may be used to locate and focus the specimen, if necessary)

Laser

Advantages

10. High intensity, giving good system sensitivity
11. Improved fluorescence resolution, since the wavelength of the excitatory light determines the size of the illuminated voxel and hence influences the overall system point spread function

Disadvantage

12. Restriction of illuminating wavelengths to 448 nm and 514 nm when using a low-cost argon ion laser (This limitation is rapidly being overcome by the development of new fluorescent dyes with large Stokes' shifts or dual wavelength emission properties that can be excited at 488 nm or 514 nm)

Unitary beam scanning

Advantages

13. Illumination of only a single voxel in the focal plane reduces light-scattering and blooming from neighbouring regions, increasing contrast
14. Low noise, high sensitivity and photometric linearity of PMT permits long integration times, allowing detection of weakly fluorescent specimens
15. Wide spectral range of PMT permits imaging in the near-infrared
16. Temporally linear data structure permits easy digitization for subsequent digital image-processing procedures
17. Images show good geometric linearity (provided the scanning system is linear)
18. Electronic zooming possible by changing the scan amplitude, or by subsequent interpolation of the digital image
19. Permits direct vertical (x,z) sectioning
20. Scanned beam systems may be added to standard compound microscopes, permitting all conventional direct full-field eyepiece imaging modes to be employed on the same specimens
21. With a transmitted light detector, scanned brightfield, darkfield, phase-contrast, Nomarski (DIC) or differential phase-contrast (DPC) images may be obtained simultaneously and in register with confocal epi-fluorescence or reflection contrast images
22. Single voxel excitation enables simultaneous dual or multiple channel imaging, without subsequent image spatial registration problems, permitting double-labelling and fluorescence emission ratio imaging

Disadvantages

23. Relatively slow scan rates, preventing real-time imaging, except on video-rate scanning systems using an acousto–optic deflector
24. Requires associated digital image processor for optimum usefulness
25. Relatively expensive

such a display, which they call a simulated fluorescence emission process. The three-dimensional image of the specimen is modelled as though it were illuminated with excitatory light from an oblique angle, and as if a surface layer a few voxels in depth emitted fluorescent light equally in all directions in response to this excitation, with an intensity proportional to the degree of excitation. This fluorescence emission is then modelled as being imaged from another defined angle, by summing the emitted light from back to front along the selected direction, the light being absorbed if it has to pass through intervening specimen voxels, giving automatic hidden feature removal in the final image. By altering the constants that model the efficiency of absorption of the excitatory light and of the fluorescence emission, the objects can be displayed as opaque or semi-transparent. It is further possible to use an 'electronic knife' to section the model at any arbitrary angle and look within. While extremely useful for the non-stereoscopic publication of 3-D data, as shown in Fig. 21, such images may, of course, themselves be made stereoscopic. The method is particularly effective for imaging solid objects such as condensed chromosomes (van der Voort *et al.* 1989; Oud *et al.* 1989).

Computer animation of 3-D confocal cellular tomographic images

The ultimate development of CSOM cellular tomography is to compute not just a single stereoscopic image pair, but an incremental series of such pairs that may be subsequently retrieved from digital memory or videotape storage and displayed in rapid succession, thus forming a stereoscopic animation sequence. If the successive stereo pairs are calculated at small incremental circumferential angles, the stereoscopically viewed specimen, upon replay, appears to rotate before one's eyes (Carlsson *et al.*

1985; White, N.S. *et al.* 1989). If, alternatively, successive image pairs are calculated at increasing distances along one axis, for instance down the z axis (Inoué and Inoué, 1986), or alternatively along the y axis for a series of transverse x,z vertical sections of an elongated structure such as an embryonic neural tube, then upon replay one will have the illusion of moving progressively along the specimen. For this latter approach to work most effectively, perspective rather than orthogonal stereoscopic projections are required, giving the viewer the impression of actually floating through the structure, like one of de Duve's 'cytonauts' (de Duve, 1984).

This technique can be further extended by displaying a series of stereo images of the same space that have been recorded at different times. Such a four-dimensional (x,y,z,t) display of a time-lapse series of confocal images collected from a three-dimensional specimen; for example, a live immunogold-labelled thymocyte undergoing capping, as described above (White, N.S. *et al.* 1989), or a living embryo in which certain cells had been specifically labelled with a fluorescent marker, would enable one to study membrane dynamics, or cellular migration during early embryonic development, with a clarity and facility hitherto impossible to contemplate.

The tumbling costs of computer workstations with powerful digital image-processing capabilities, and the availability of novel digital storage and stereoscopic image display hardware, and of optical disc video recorders, now makes such stereoscopic animation of CSOM images increasingly achievable. Confocal scanning optical microscopy thus brings closer an era of cellular visualization in which it will be possible to stereoscopically view, rotate, quantify and transform blur-free images of cellular ultrastructure with an ease akin to that exemplified by recent advances in the fields of whole body medical imaging on the one hand and molecular graphics on the other.

Conclusion

Arguably the most significant advance in optical microscopy in this decade, confocal scanning optical microscopy is a powerful new tool for the cellular and developmental biologist, with the benefits (and disadvantages) listed in Table 1. It is entirely compatible with the conventional range of light-microscopic techniques, and, at least in scanned beam instruments, may indeed be applied to the same specimens on the same optical microscope stage. In many ways it complements modern video-enhanced light-microscopic (VELM) techniques, described elsewhere (Shotton, 1987, 1988*a*). Its chief advantage is its ability to generate non-invasive optical sections of labelled specimens with a virtual absence of out-of-focus blur. While the extent of its future applications is hard to predict, its potential for biological research appears enormous, particularly for analysis of the three-dimensional organization of cellular macromolecules and organelles, for fluorescence ratio imaging studies of physiological parameters within single cells, and for neurobiological, pathological and developmental studies of fixed or living tissues and organisms, where it is desirable to obtain clear images many micrometres below the surface of the tissue under examination.

I am most grateful to John White, Brad Amos and Andrew Dixon (of Bio-Rad Lasersharp Ltd) for the opportunity to use a pre-production model of the Lasersharp MRC-500 confocal scanning fluorescence microscope, and for stimulating discussions and advice concerning CSOM. I am also greatly indebted to all those who have kindly supplied micrographs of their own work to illustrate this review, and to Nick White, David Agard, Hans Tanke and Brad Amos for their critical readings of earlier drafts of the manuscript. A brief article covering some of the topics contained in this review has recently appeared in the Proceedings of the Royal Microscopical Society (Shotton, 1988*b*), and common material is included here with permission of that Society. This review was written, in part, during the tenure of a CIBA-GEIGY Senior Fellowship.

References

AGARD, D. A. (1984). Optical sectioning microscopy: cellular architecture in three dimensions. *A. Rev. Biophys. Bioengng* **13**, 191–219.

AGARD, D. A., HIRAOKA, Y., SHAW, P. J. AND SEDAT, J. W. (1989). Fluorescence microscopy in three dimensions. In *Fluorescence Microscopy of Living Cells in Culture: B. Quantitative Fluorescence Microscopy – Imaging and Spectroscopy* (Taylor, D.L. and Wang, Y.-L., eds) *Methods in Cell Biology* vol. **30**. New York: Academic Press.

AMOS, W. B., WHITE, J. G. AND FORDHAM, M. (1987). Use of confocal imaging in the study of biological structures. *Appl. Opt.* **26**, 3239–3243.

ASH, E. A. (1980). *Scanned Image Microscopy*, London: Academic Press.

AWAMURA, D., ODE, T. AND YONEZAWA, M. (1987). Color laser microscope. *Proc. Soc. Photo-Optical Instrument. Eng. (SPIE)* **765**, 53–60.

BAAK, J. P. A., THUNNISSEN, F. B. J. M., OUDEJANS, C. B. M. AND SCHIPPER, N. W. (1987). Potential clinical uses of laser scan microscopy. *Appl. Opt.* **26**, 3413–3416.

BARTELS, P. H., BUCHROEDER, R. A., HILLMAN, D. W., JONAS, J., KESSLER, D., SHOEMAKER, R. L., SHACK, R. V., TOWNER, D. AND VUKOBRATOVICH, D. (1981). Ultrafast laser scanner microscope design and construction. *J. analyt. quant. Cytol.* **3**, 55–61.

BARTELS, P. H., GRAHAM, W. K., PAPLANUS, S. AND WIED, G. L. (1987). Knowledge engineering in quantitative histopathology. *Appl. Opt.* **26**, 3330–3337.

BECK, K. AND BEREITER-HAHN, J. (1981). Evaluation of reflection interference contrast images of living cells. *Microscopica Acta* **84**, 153–178.

BEESLEY, J. (1985). Colloidal gold: a new revolution in marking cytochemistry. *Proc R. microsc. Soc.* **20**, 187–196 and 255–256.

BERTERO, M., BRIANZI, B. AND PIKE, E. R. (1987). Super-resolution in confocal scanning microscopy. *Inverse Problems* **3**, 195–212.

BORN, M. AND WOLF, E. (1975). *Principles of Optics*, pp. 437–442. London: Pergamon Press.

BOYDE, A. (1985*a*). The tandem scanning reflected light microscope. Part 2: pre-Micro '84 applications at UCL. *Proc. R. Microsc. Soc.* **20**, 131–139.

BOYDE, A. (1985*b*). Stereoscopic images in confocal (tandem scanning) microscopy. *Science* **230**, 1270–1272.

BOYDE, A. (1986). Applications of tandem scanning reflected light microscopy and three-dimensional imaging. *Ann. N.Y. Acad. Sci.* **483**, 428–439.

BOYDE, A. (1987). Colour-coded stereo images from the tandem scanning reflected light microscope (TSRLM). *J. Microsc.* **146**, 137–142.

BOYDE, A., HADRAVSKY, M., PETRAN, M., WATSON, T. F., JONES, S. J., MARTIN, L. B. AND REID, S. A. (1986). Tandem scanning

reflected light microscopy: how it works and applications. *Proc. 44th Ann. Meeting Electron Microscop. Soc. Am.* (ed. G.W.Bailey), pp. 84–87. San Francisco: San Francisco Press Inc.

BOYDE, A., PETRAN, M. AND HADRAVSKY, M. (1983). Tandem scanning reflected light microscopy of internal features in whole bone and tooth samples. *J. Microsc.* **132**, 1–7.

BRAKENHOFF, G. J. (1978). Imaging modes in confocal scanning light microscopy (CSLM). *Proc. ICO-11 Conference* (Madrid, Spain), pp. 219–222.

BRAKENHOFF, G. J. (1979). Imaging modes in confocal scanning light microscopy (CSLM). *J. Microsc.* **117**, 233–242.

BRAKENHOFF, G. J. (1989). Confocal microscopy, past, present and some thoughts on the future. *Proc. 1st Int. Conf. Confocal Microscopy* (Amsterdam, March 1989).

BRAKENHOFF, G. J., BINNERTS, J. S. AND BARENDS, P. (1981). High resolution confocal scanning light microscopy (CSLM) as applied to living biological specimens. *Scanning Electron Microsc.* **II**, 131–138, 158.

BRAKENHOFF, G. J., BINNERTS, J. S. AND WOLDRINGH, C. L. (1980). Developments in high resolution confocal scanning light microscopy (CSLM). In *Scanned Image Microscopy* (ed. E.A. Ash), pp. 183–200. London: Academic Press.

BRAKENHOFF, G. J., BLOM, P. AND BAKKER, B. (1978). Confocal scanning light microscopy with high aperture optics. *Proc. ICO-11 Conference* (Madrid, Spain), pp. 215–218.

BRAKENHOFF, G. J., BLOM, P. AND BARENDS, P. (1979). Confocal scanning light microscopy with high aperture lenses. *J. Microsc.* **117**, 219–232.

BRAKENHOFF, G. J., VAN DER VOORT, H. T. M., VAN SPRONSEN, E. A., LINNEMANS, W. A. M. AND NANNINGA, N. (1985). Three-dimensional chromatin distribution in neuroblastoma nuclei shown by confocal scanning laser microscopy. *Nature, Lond.* **317**, 748–749.

BRAKENHOFF, G. J., VAN DER VOORT, H. T. M., VAN SPRONSEN, E. A. AND NANNINGA, N. (1986). Three-dimensional imaging by confocal scanning fluorescence microscopy. *Ann. N.Y. Acad. Sci.* **483**, 405–415.

BRAKENHOFF, G. J., VAN DER VOORT, H. T. M., VAN SPRONSEN, E. A. AND NANNINGA, N. (1989). Three-dimensional imaging in fluorescence by confocal scanning microscopy. *J. Microsc.* **153**, 151–159.

BREARLEY, M. A. (1985). Prototype scanning laser microscope. *J. Inst. Electronic Radio Eng.* **55**, 162–164.

BRIGHT, G. R., FISHER, G. W., ROGOWSKA, J. AND TAYLOR, D. L. (1987). Fluorescence ratio imaging microscopy: temporal and spatial measurements of cytoplasmic pH. *J. Cell Biol.* **104**, 1019–1033.

CARLSSON, K. AND ÅSLUND, N. (1987). Confocal imaging for 3-D digital microscopy. *Appl. Opt.* **26**, 3232–3238.

CARLSSON, K., DANIELSSON, P. E., LENZ, R., LILJEBÖRG, A., MAJLOF, L. AND ÅSLUND, N. (1985). Three-dimensional microscopy using a confocal laser scanning microscope. *Optics Lett.* **10**, 53–55.

CARLSSON, K. AND LILJEBÖRG, A. (1989). A confocal laser microscope scanner for the digital recording of optical serial sections. *J. Microsc.* **153**, 171–180.

CASTLEMAN, K. R. (1979). *Digital Image Processing*. Englewood Cliffs, New Jersey: Prentice-Hall.

CORLE, T. R., CHOU, C. H. AND KINO, G. S. (1986). Depth response of confocal optical microscopes. *Optics Lett.* **11**, 770–772.

CORNELESE-TEN VELDE, I., BONNET, J., TANKE, H. J. AND PLOEM, J. S. (1988). Reflection contrast microscopy. Visualization of (peroxidase-generated) diaminobenzidine polymer products and its underlying optical phenomena. *Histochemistry* **89**, 141–150.

COX, I. J. (1982). Microprocessors in scanning microscopy. *Software Microsystems* **2**, 15–18.

COX, I. J. (1984). Scanning optical fluorescence microscopy. *J. Microsc.* **133**, 149–154.

COX, I. J. AND SHEPPARD, C. J. R. (1983*a*). Scanning optical microscope incorporating a digital framestore and microcomputer. *Appl. Opt.* **22**, 1474–1478.

COX, I. J. AND SHEPPARD, C. J. R. (1983*b*). Digital image processing of confocal images. *Image Vision Comput.* **1**, 52–56.

COX, I. J., SHEPPARD, C. J. R. AND WILSON, T. (1982*a*). Super-resolution by confocal fluorescence microscopy. *Optik* **60**, 391–396.

COX, I. J., SHEPPARD, C. J. R. AND WILSON, T. (1982*b*). Reappraisal of arrays of concentric annuli as superresolving filters. *J. opt. Soc. Am.* **72**, 1287–1291.

COX, I. J., SHEPPARD, C. J. R. AND WILSON, T. (1982*c*). Improvement in resolution by nearly confocal microscopy. *Appl. Opt.* **21**, 778–781.

CREMER, C. AND CREMER, T. (1978). Considerations on a laser-scanning-microscope with high resolution and depth of field. *Microscopica Acta* **81**, 31–44.

CRUZ-ORIVE, L. M. (1987). Particle number can be estimated using a dissector of unknown thickness: the selector. *J. Microsc.* **145**, 121–142.

DEBIASIO, R., BRIGHT, G. R., ERNST, L. A., WAGGONER, A. S. AND TAYLOR, D. L. (1987). Five-parameter fluorescence imaging: wound healing of living Swiss 3T3 cells. *J. Cell Biol.* **105**, 1613–1622.

DE BRABANDER, M., GEUENS, G., NUYDENS, R., MOEREMANS, M. AND DE MEY, J. (1985). Probing microtubule-dependent intracellular motility with nanometer particle video ultramicroscopy. *Cytobios* **43**, 273–283.

DE BRABANDER, M., NUYDENS, R., GEUENS, G., MOEREMANS, M. AND DE MEY, J. (1986). The use of submicroscopic gold particles combined with video contrast enhancement as a simple molecular probe for the living cell. *Cell Motil. Cytoskel.* **6**, 105–113.

DE DUVE, C. (1984). *A Guided Tour of the Living Cell*. New York: Scientific American Library/W.H. Freeman and Co.

DE MEY, J. (1983). Colloidal gold probes in immunocytochemistry. In *Immunocytochemistry* (ed. J.M. Polak and S. van Noorden), pp. 82–112. Bristol, London, Boston: Wright PSG.

DEINET, W., LINKE, M., MÜLLER, R. AND SANDER, I. (1983). Laser-scanning microscopy mit automatischer fokussierung. *Microscopica Acta* **87**, 129–138.

DIXON, A. J. AND MARTIN, J. B. (1986). Design of a confocal laser scanning optical microscope. *Beitr. electronenmikroskop. Direktabb. Oberfl.* **19**, 139–151.

DRAAIJER, A. AND HOUPT, P. M. (1988). A standard video-rate confocal laser-scanning reflection and fluorescence microscope. *Scanning* **10**, 139–145.

EGGER, M. D. AND PETRAN, M. (1967). New reflected-light microscopy for viewing unstained brain and ganglion cells. *Science* **157**, 305–307.

FINE, A., AMOS, W. B., DURBIN, R. M. AND MCNAUGHTON, P. A. (1988). Confocal microscopy: applications in neurobiology. *Trends Neurosci.* **11**, 346–351.

GEERTS, H., DE BRABANDER, M., NUYDENS, R., GEUENS, S., MOEREMANS, M., DE MEY, J. AND HOLLENBECK, P. (1987). Nanovid tracking: a new automatic method for the study of mobility in living cells based on colloidal gold and video microscopy. *Biophys. J.* **52**, 775–782.

GINGELL, D. AND TODD, I. (1979). Interference reflection microscopy. A quantitative theory for image interpretation and its application to cell–substratum separation measurements. *Biophys. J.* **26**, 507–526.

GOLDSTEIN, S. (1989). A no-moving-parts video rate laser beam scanning type 2 confocal reflected/transmission microscope. *J. Microsc.* **153**, RP1–RP2.

GRUENBAUM, Y., HOCHSTRASSER, M., MATHOG, D., SAUMWEBER, H., AGARD, D. A. AND SEDAT, J. W. (1984). Spatial organization of the *Drosophila* nucleus: a three-dimensional cytogenetic study. *J. Cell Sci. Suppl.* 1, 223–234.

GRYNKIEWICZ, G., POENIE, M. AND TSIEN, R. Y. (1985). A new generation of Ca^{2+} indicators with greatly improved fluorescence properties. *J. biol. Chem.* **260**, 3440–3450.

HAMILTON, D. K. AND MATTHEWS, H. J. (1985). The confocal interference microscope as a surface profilometer. *Optik* **71**, 31–34.

HAMILTON, D. K. AND SHEPPARD, C. J. R. (1982). A confocal interference microscope. *Optica Acta* **29**, 1573–1577.

HAMILTON, D. K. AND SHEPPARD, C. J. R. (1984). Differential phase contrast in scanning optical microscopy. *J. Microsc.* **133**, 27–39.

HAMILTON, D. K., SHEPPARD, C. J. R. AND WILSON, T. (1984). Improved imaging of phase gradients in scanning optical microscopy. *J. Microsc.* **135**, 19–25.

HAMILTON, D. K. AND WILSON, T. (1982*a*). Surface profile measurement using the confocal microscope. *J. appl. Phys.* **53**, 5320–5322.

HAMILTON, D. K. AND WILSON, T. (1982*b*). Three-dimensional surface measurement using the confocal scanning microscope. *Appl. Phys.* **27**, 211–213.

HAMILTON, D. K. AND WILSON, T. (1984*a*). Two-dimensional phase imaging in the scanning optical microscope. *Appl. Opt.* **23**, 348–352.

HAMILTON, D. K. AND WILSON, T. (1984*b*). Edge enhancement in scanning optical microscopy by differential detection. *J. opt. Soc. Am. (A)* **1**, 322–323.

HAMILTON, D. K. AND WILSON, T. (1986). Scanning optical microscopy by objective lens scanning. *J. Phys. E: Sci. Instrum.* **19**, 52–54.

HAMILTON, D. K., WILSON, T. AND SHEPPARD, C. J. R. (1981). Experimental observations of the depth-discrimination properties of scanning microscopes. *Optics Lett.* **6**, 625–626.

HAUGLAND, R. (1987). A variety of new fluorescence probes. *Cytometry Suppl.* **1**, 31.

HAUGLAND, R. (1988). Dual emission and dual excitation pH indicators: SNARFs and SNAFLs. *Bioprobes* **8**, 2–4 (Published by Molecular Probes Inc.).

HEGEDUS, Z. S. AND SARAFIS, V. (1986). Superresolving filters in confocal scanned imaging systems. *J. opt. Soc. Am.* **3**, 1892–1896.

HIRAOKA, Y., SEDAT, J. W. AND AGARD, D. A. (1987). The use of a charge-coupled device for quantitative optical microscopy of biological structures. *Science* **238**, 36–41.

HORIKAWA, Y., YAMAMOTO, M. AND DOSAKA, S. (1987). Laser scanning microscope: differential phase images. *J. Microsc.* **148**, 1–10.

HOWARD, V., REID, S., BADDERLEY, A. AND BOYDE, A. (1985). Unbiased estimation of particle density in the tandem scanning reflected light microscope. *J. Microsc.* **138**, 203–212.

HYMAN, A. A. AND WHITE, J. G. (1987). Determination of cell division axes in the early embryogenesis of *Caenorhabditis elegans*. *J. Cell Biol.* **105**, 2123–2135.

INOUÉ, S. AND INOUÉ, T. D. (1986). Computer-aided stereoscopic video reconstruction and serial section display from high-resolution light-microscope optical sections. *Ann. N.Y. Acad. Sci.* **483**, 392–404.

INOUÉ, S., INOUÉ, T. D. AND ELLIS, G. W. (1985). Rapid stereoscopic display of microtubule distribution by a video-processed optical sectioning system. *J. Cell Biol.* **101**, 146a.

ISAACSON, M., BETZIG, E., HAROOTUNIAN, A. AND LEWIS, A. (1986). Scanning optical microscopy at $\lambda/10$ resolution using near-field imaging methods. *Ann. N.Y. Acad. Sci.* **483**, 448–456.

JEACOCKE, R. (1989). Confocal microscopy of skeletal muscle. *Proc. 1st Int. Conf. Confocal Microscopy* (Amsterdam, March 1989).

KALISCH, W.-E., WHITMORE, T. AND SIEGAL, A. (1985). Laser scanning microscopy of surface spread polytene chromosomes. *J. Microsc.* **137**, 217–224.

KOCH, G. L. E., MACER, D. R. J. AND SMITH, M. J. (1987). Visualization of the intact endoplasmic reticulum by immunofluorescence with antibodies to the major ER glycoprotein, endoplasmin. *J. Cell Sci.* **87**, 535–542.

LANDEGENT, J. E., JANSEN IN DE WAL, N., PLOEM, J. S. AND VAN DER PLOEG, M. (1985). Sensitive detection of hybridocytochemical results by means of reflection-contrast microscopy. *J. Histochem. Cytochem.* **33**, 1241–1246.

LEWIN, R. (1985). New horizons for light microscopy. *Science* **230**, 1258–1262.

LEWIS, A., ISSACSON M., HARTOOTUNIAN, A. AND MURAY, A. (1984).Development of a 500 Å spatial resolution light microscope. I: Light is efficiently transmitted through $\lambda/16$ diameter apertures. *Ultramicroscopy* **13**, 227–232.

MINSKY, M. (1957). U.S. Patent no. 3013467. Microscopy Apparatus, Dec. 19, 1961 (Filed Nov. 7, 1957).

MINSKY, M. (1988). Memoir on inventing the confocal scanning microscope. *Scanning* **10**, 128–138.

MUNRO, S. AND PELHAM, H. R. B. (1987). A C-terminal signal prevents secretion of luminal ER proteins. *Cell* **48**, 899–907.

NEDERLOF, P. M., ROBINSON, D., ABUKNESHA, R., WIEGANT, J., HOPMAN, A. H. N., TANKE, H. J. AND RAPP, A. K. (1989). Three color fluorescence *in situ* hybridization for the simultaneous detection of multiple nucleic acid sequences in interphase nuclei and chromosomes. *Cytometry* **10**, 20–27.

OSBORN, M., BORN, T., KOITSCH, H.-J. AND WEBER, K. (1978). Stereo-immunofluorescence microscopy. I: Three-dimensional arrangement of microfilaments, microtubules and tonofilaments. *Cell* **14**, 477–488.

OUD, J. L., MANS, A., BRAKENHOFF, G. J., VAN DER VOORT, H. T. M., VAN SPRONSEN, E. A. AND NANNINGA, N. (1989). Three-dimensional chromosome arrangement of *Crepis capillaris* in mitotic prophase and anaphase as studied by confocal scanning laser microscopy. *J. Microsc.* **92**, 329–339.

PETERS, R. (1985). Measurement of membrane transport in single cells by fluorescence microphotolysis. *Trends Biochem. Sci.* **10**, 223–227.

PETRAN, M., HADRAVSKY, M., BENES, J. AND BOYDE, A. (1986). *In vitro* microscopy using the tandem scanning light microscope. *Ann. N.Y. Acad. Sci.* **483**, 440–447.

PETRAN, M., HADRAVSKY, M., BENES, J., KUCERA, R. AND BOYDE, A. (1985*a*). The tandem scanning reflected light microscope: Part 1: the principle, and its design. *Proc. R. Microsc. Soc.* **20**, 125–129.

PETRAN, M., HADRAVSKY, M., BOYDE, A. AND MUELLER, M. (1985*b*). Tandem scanning reflected light microscopy. In *Science of Biological Specimen Preparation for Microscopy and Microanalysis* (ed. M. Mueller, R.P. Becker, A. Boyde and J.J. Wolosewick), pp. 85–94. AMF O'Hare (Chicago): SEM Inc.

PETRAN, M., HADRAVSKY, M., EGGAR, M. D. AND GALAMBOS, R. (1968). Tandem-scanning reflected-light microscopy. *J. opt. Soc. Am.* **58**, 661–664.

PIKE, E. R., BERTERO, M. AND DE MOL, C. (1987). A new inversion procedure for confocal scanning microscopy and other bandlimited signal processing problems. *Proc. Soc. Photo-Optical Instrument. Eng. (SPIE)* **813**, 159–160.

PILLER, H. (1959). Enhancement of contrast in reflected-light microscopy. *Zeiss Werkzeitschrift* **34**, 87.

PLOEM, J. S. (1975). Reflection-contrast microscopy as a tool for investigation of the attachment of living cells to a glass surface. In *Mononuclear Phagocytes in Immunity, Infection and Pathology*. (ed. R. van Furth), pp. 405–421. Oxford: Blackwell.

PLOEM, J. S. (1986). New instrumentation for sensitive image analysis of fluorescence in cells and tissues. In *Applications of Fluorescence in the Biomedical Sciences* (ed. D.L. Taylor, A.S. Waggoner, F. Lamb, R.F Murphy and R.R. Birge), pp. 289–300. New York: A.R. Liss, Inc.

PLOEM, J. S. (1987). Laser scanning fluorescence microscopy. *Appl. Opt.* **26**, 3226–3231.

RAWLINS, D. J. AND SHAW, P. J. (1988). Three-dimensional organization of chromosomes of *Crepis capillaris* by optical tomography. *J. Cell Sci.* **91**, 401–414.

REIMER, L., EGELKAMP, S. AND VERST, M. (1987). Lock-in technique for depth-profiling and magneto-optical Kerr effect imaging in scanning optical microscopy. *Scanning* **9**, 17–25.

ROBERT-NICOUD, M., ARNDT-JOVIN, D., SCHORMANN, T. AND JOVIN, T. M. (1989). 3-D imaging of cells and tissues using confocal laser scanning microscopy and digital processing. *Eur. J. Cell Biol.* **48** (Suppl. **25**), 49–52.

RUSS, J. C. (1989). Direct 3-D imaging of pore location in ceramics using confocal light and acoustic microscopes. *Proc. 1st Int. Conf. Confocal Microsc.* (Amsterdam, March 1989).

SCHORMANN, T., ROBERT-NICOUD, T. M. AND JOVIN, T. M. (1989). Improved stereovisualisation method for confocal laser scanning microscopy. *Eur. J. Cell Biol.* **48** (Suppl. **25**), 53–54.

SHAW, P. J., AGARD, D. A., HIRAOKA, Y. AND SEDAT, J. W. (1989). Tilted view reconstruction in optical microscopy: three-dimensional reconstruction of *Drosophila melanogaster* embryo nuclei. *Biophys. J.* **55**, 101–110.

SHEPPARD, C. J. R. (1980). Imaging modes of scanning optical microscopy. In *Scanned Image Microscopy* (ed. E.A. Ash), pp. 201–225. London: Academic Press.

SHEPPARD, C. J. R. (1982). Applications of scanning confocal microscopy. *Proc. Soc. Photo-Optical Instrument. Eng. (SPIE)* **368**, 88–95.

SHEPPARD, C. J. R. (1986*a*). The spatial frequency cut-off in three-dimensional imaging. *Optik* **72**, 131–133.
SHEPPARD, C. J. R. (1986*b*). Scanned imagery. *J. Phys. D: appl. Phys.* **19**, 2077–2084.
SHEPPARD, C. J. R. (1987). Scanning optical microscopy. *Adv. Opt. Electron Microsc.* **10**, 1–98.
SHEPPARD, C. J. R. (1988). Super-resolution in confocal imaging. *Optik* **80**, 53–54.
SHEPPARD, C. J. R. (1989). Axial resolution of confocal fluorescence microscopy. *J. Microsc.* **154**, 237–241.
SHEPPARD, C. J. R. AND CHOUDHURY, A. (1977). Image formation in the scanning microscope. *Optica Acta* **24**, 1051–1073.
SHEPPARD, C. J. R. AND CHOUDHURY, A. (1978). The image of a bar-pattern in the scanning microscope. *Optik* **51**, 361–368.
SHEPPARD, C. J. R. AND COGGISWELL, C. J. (1989). Three dimensional imaging in confocal microscopy. *Proc. 1st Int. Conf. Confocal Microsc.* (Amsterdam, March 1989).
SHEPPARD, C. J. R. AND HAMILTON, D. K. (1983). High resolution stereoscopic imaging. *Appl. Opt.* **22**, 886–887.
SHEPPARD, C. J. R. AND HAMILTON, D. K. (1984). Edge enhancement by defocusing of confocal images. *Optica Acta* **31**, 723–727.
SHEPPARD, C. J. R., HAMILTON, D. K. AND COX, I. J. (1983). Optical microscopy with extended depth of field. *Proc. R. Soc. Lond. A* **387**, 171–186.
SHEPPARD, C. J. R. AND HEATON, J. M. (1984). Confocal microscopy of straight edges and surface steps. *Optik* **68**, 371–380.
SHEPPARD, C. J. R. AND WILSON, T. (1978*a*). Image formation in scanning microscopes with partially coherent source and detector. *Optica Acta* **25**, 315–325.
SHEPPARD, C. J. R. AND WILSON, T. (1978*b*). Depth of field in the scanning microscope. *Optics Lett.* **3**, 115–117.
SHEPPARD, C. J. R. AND WILSON, T. (1978*c*). The theory of scanning microscopy with Gaussian pupil functions. *J. Microsc.* **114**, 179–186.
SHEPPARD, C. J. R. AND WILSON, T. (1981). The theory of the direct-view confocal microscope. *J. Microsc.* **124**, 107–117.
SHEPPARD, C. J. R. AND WILSON, T. (1986*a*). On the equivalence of scanning and conventional microscopy. *Optik* **73**, 39–43.
SHEPPARD, C. J. R. AND WILSON, T. (1986*b*). Reciprocity and equivalence in scanning microscopes. *J. opt. Soc. Am. (A)* **3**, 755–756.
SHOEMAKER, R. L., BARTELS, P. H., HILLMAN, D. W., JONAS, J., KESSLER, D., SHACK, R. V. AND VUKOBRATOVICH, D. (1982). An ultrafast laser scanner microscope for digital image analysis. *IEEE Trans. biomed. Eng.* **BME-29**, 82–91.
SHOTTON, D. M. (1987). The current renaissance in light microscopy. I. Dynamic studies of living cells by video enhanced contrast microscopy. *Proc. R. Microsc. Soc.* **22**, 37–44.
SHOTTON, D. M. (1988*a*). Review: Video enhanced light microscopy and its applications in cell biology. *J. Cell Sci.* **89**, 129–150.
SHOTTON, D. M. (1988*b*). The current renaissance in light microscopy. II. Blur-free optical sectioning of biological specimens by confocal scanning fluorescence microscopy. *Proc. R. Microsc. Soc.* **23**, 289–297.
SHUMAN, H. (1988). Contrast in confocal scanning microscopy with a finite detector. *J. Microsc.* **149**, 67–71.
SMITH, J., JONGENELEN, J., LAMERS, W. H., LOS, J. A. AND STRACKEE, J. (1989). Octree representation for 3D image analysis. *Eur. J. Cell Biol.* **48** (Suppl. **25**), 97–98.
STELZER, E. H. K. AND WIJNAENDTS VAN RESANDT, R. W. (1986). Applications of fluorescence microscopy in three dimensions: microtomoscopy. *Biostereometrics: Proc. Soc. Photo-Optical Instrument. Eng. (SPIE)* **602**, 63–70.
SUZUKI, T. AND HORIKAWA, Y. (1986). Development of a real-time scanning laser microscope for biological use. *Appl. Opt.* **25**, 4115–4121.
TAKAMATSU, T. AND FUJITA, S. (1988). Microscopic tomography by laser scanning microscopy and its three-dimensional reconstruction. *J. Microsc.* **149**, 167–174.
TANASUGARN, L., MCNEIL, P., REYNOLDS, G. AND TAYLOR, D. L. (1984). Microspectrofluorimetry by digital image processing: measurement of cytoplasmic pH. *J. Cell Biol.* **98**, 717–724.
TSIEN, R. Y. AND POENIE, M. (1986). Fluorescence ratio imaging: a new window into intracellular ionic signaling. *Trends Biochem. Sci.* **11**, 450–455.
TUCKER, J. H. (1987). Scanning cytometry for fast ploidy measurement and cell featuring in cancers. *Cytometry* Suppl. **1**, 18.
VAN DER VOORT, H. T. M. AND BRAKENHOFF, G. J. (1989). A numerical analysis of the 3-D image formation in a high numerical aperture confocal fluorescence microscope. *Proc. 1st Int. Conf. Confocal Microsc.* (Amsterdam, March 1989).
VAN DER VOORT, H. T. M., BRAKENHOFF, G. J. AND BAARSLAG, M. W. (1989). Three-dimensional visualization methods for confocal microscopy. *J. Microsc.* **153**, 123–132.
VAN DER VOORT, H. T. M., BRAKENHOFF, G. J. AND JANSSEN, G. C. A. M. (1988). Determination of the 3-dimensional optical properties of a confocal scanning laser microscope. *Optik* **78**, 48–53.
VAN DER VOORT, H. T. M., BRAKENHOFF, G. J., JANSSEN, G. C. A. M., VALKENBURG, J. A. C. AND NANNINGA, N. (1987). Confocal scanning fluorescence and reflection microscopy: measurements of the 3-D image formation and applications in biology. *Proc. Soc. Photo-Optical Instrument. Eng. (SPIE)* **809**, 138–143.
VAN DER VOORT, H. T. M., BRAKENHOFF, G. J., VALKENBURG, J. A. C. AND NANNINGA, N. (1985). Design and use of a computer controlled confocal microscope for biological applications. *Scanning* **7**, 66–78.
VAN GEEL, F., SMITH, B. W., NICOLAISSEN, B. AND WINEFORDNER, J. D. (1984). Epi-fluorescence microscopy with a pulsed nitrogen tunable dye laser source. *J. Microsc.* **133**, 141–148.
VAN MEER, G., STELZER, E. H. K., WIJNAENDTS VAN RESANDT, R. W. AND SIMONS, K. (1987). Sorting of sphingolipids in epithelial (Madin-Darby canine kidney) cells. *J. Cell Biol.* **105**, 1623–1635.
VERSCHUEREN, H. (1985). Interference reflection contrast microscopy in cell biology: methodology and applications. *J. Cell Sci.* **75**, 279–301.
WHITE, J. G. AND AMOS, W. B. (1987). Confocal microscopy comes of age. *Nature, Lond* **328**, 183–184.
WHITE, J. G., AMOS, W. B. AND FORDHAM, M. (1987). An evaluation of confocal versus conventional imaging of biological structure by fluorescence light microscopy. *J. Cell Biol.* **105**, 41–48.
WHITE, N. S., DIXON, A., DOE, E. AND SHOTTON, D. M. (1987). Scanning optical microscopy of biological specimens. *Proc. R. Microsc. Soc.* **22**, 99.
WHITE, N. S., LACKIE, P. M. AND SHOTTON, D. M. (1989). Stereoscopic animation of three-dimensional data sets collected by confocal reflection contrast scanning optical microscopy from capping thymocytes bearing immunogold-labelled antigens. *Proc. 1st Int. Conf. Confocal Microsc.* (Amsterdam, March 1989).
WIJNAENDTS VAN RESANDT, R. W., MARSMAN, H. J. B., KAPLAN, R., DAVOUST, J., STELZER, E. H. K. AND STRICKER, R. (1985). Optical fluorescence microscopy in three dimensions: microtomoscopy. *J. Microsc.* **138**, 29–34.
WILKE, V. (1985). Optical scanning microscopy – the laser scan microscope. *Scanning* **7**, 88–96.
WILLIAMS, P., MCLAUGHLIN, S. R. AND LEARY, J. F. (1987). MEDUSA – A *m*ulticolour *e*xcitation *d*ye laser for *u*ser *a*pplications. *Cytometry* Suppl. **1**, 24.
WILSON, T. (1980). Imaging properties and applications of scanning optical microscopes. *Appl. Phys.* **22**, 119–125.
WILSON, T. (1981). Images of phase edges in conventional and scanning optical microscopy. *Appl. Opt.* **20**, 3238–3244.
WILSON, T. (1985*a*). Scanning optical microscopy. *Scanning* **7**, 79–87.
WILSON, T. (1985*b*). Scanning optical microscopy. In *Advances in Microscopy* (ed. Cowden, R.R. and Harrison, F.W.), pp. 103–113. New York: A.R. Liss.
WILSON, T. (1986). Confocal light microscopy. *Ann. N.Y. Acad. Sci.* **483**, 416–427.
WILSON, T. (1988). Enhanced differential phase contrast imaging in scanning microscopy using a quatrant detector. *Optik* **80**, 167–170.
WILSON, T. (1989). Three-dimensional imaging in confocal systems. *J. Microsc.* **153**, 161–169.
WILSON, T. (1989). Optical sectioning in confocal fluorescent microscopes. *J. Microsc.* **154**, 143–156.

WILSON, T. AND CARLINI, A. R. (1987*a*). Size of the detector in confocal imaging systems. *Optics Lett.* **12**, 227–229.
WILSON, T. AND CARLINI, A. R. (1987*b*). Depth discrimination criteria in confocal systems. *Optik* **76**, 164–166.
WILSON, T. AND CARLINI, A. R. (1988). Three-dimensional imaging in confocal imaging systems with finite sized detectors. *J. Microsc.* **149**, 51–66.
WILSON, T. AND CARLINI, A. R. (1989). The effect of aberrations on the axial response of confocal systems. *J. Microsc.* **154**, 243–256.
WILSON, T., CARLINI, A. R. AND HAMILTON, D. K. (1986*a*). Images of thick step objects in confocal scanning microscopy by axial scanning. *Optik* **73**, 123–126.
WILSON, T., CARLINI, A. R. AND SHEPPARD, C. J. R. (1985). Phase contrast microscopy by nearly full illumination. *Optik* **70**, 166–169.
WILSON, T., GANNAWAY, J. N. AND JOHNSON, P. (1980). A scanning optical microscope for the inspection of semiconductor materials and devices. *J. Microsc.* **118**, 309–314.
WILSON, T. AND HAMILTON, D. K. (1982). Dynamic focussing in the confocal scanning microscope. *J. Microsc.* **128**, 139–143.
WILSON, T. AND HAMILTON, D. K. (1983). Differential amplitude contrast imaging in the scanning optical microscope. *Appl. Phys.* B **32**, 187–191.
WILSON, T. AND HAMILTON, D. K. (1984). Difference confocal scanning microscopy. *Optica Acta* **31**, 453–465.
WILSON, T. AND HAMILTON, D. K. (1985). Dark-field scanning optical microscopy. *Optik* **71**, 23–26.
WILSON, T., MCCABE, E. M. AND HAMILTON, D. K. (1986*b*). A new method for displaying low-contrast optical-beam-induced contrast images in the scanning optical microscope. *J. Appl. Phys.* **59**, 702–703.
WILSON, T. AND SHEPPARD, C. J. R. (1984). *Theory and Practice of Scanning Optical Microscopy*. London: Academic Press.
WILSON, T. AND SHEPPARD, C. J. R. (1985). Imaging of birefringent objects in scanning microscopes. *Appl. Opt.* **24**, 2081–2084.
XIAO, G. Q., CORLE, T. R. AND KINO, G. S. (1988). Real-time confocal scanning optical microscope. *Applied Phys. Lett.* **53**, 716–718.
XIAO, G. Q. AND KINO, G. S. (1987). A real-time confocal scanning optical microscope. *Proc. 4th Int. Symp. Optical and Optoelectronic Applied Science and Engineering*, The Hague, Netherlands.
YOUNG, M. R., DAVIES, R. E., PIKE, E. R. AND WALKER, J. G. (1989). Superresolution in confocal microscopy: experimental confirmation in the 1D coherent and incoherent cases. *Proc. 1st Int. Conf. Confocal Microscopy* (Amsterdam, March 1989).

(*Received 25 May 1989 – Accepted 14 July 1989*)